EXPERIMENTAL FRAGILITY ANALYSIS OF ALUMINUM STORM PANELS SUBJECT TO WINDBORNE DEBRIS

A Thesis

Submitted to the Graduate Faculty of the
Louisiana State University and
Agricultural and Mechanical College
in partial fulfillment of the
requirements for the degree of
Master of Science in
Civil Engineering

in

The Department of Civil and Environmental Engineering

by
Taylor Claude Alphonso
B.S., University of Louisiana at Lafayette, 2011
May 2013

This work is sincerely dedicated to my parents. They have been my driving force by my side through my entire educational career. I owe any and all success to them.

ACKNOWLEDGMENTS

First and foremost, I would like to express my gratitude towards my parents, Glenda and Kent Alphonso, for the encouragement they have given me throughout not just my educational career, but also my entire life. Without their support, the success I have achieved would not have been possible. I would like to thank Dr. Barbato for not only providing me with the opportunity to pursue my graduate studies at LSU, but also for the outstanding guidance, extremely long hours, and dedication to my focus. I would also like to sincerely thank the other members of my advisory committee, Dr. Ayman Okeil and Dr. Steve Cai, for providing me with useful advice and assistance as needed throughout my course of study, and also for serving on my examination committee. With no hesitation, both gentlemen agreed to be part of my committee while still handling the everyday stresses of being an educator. This is much appreciated. Lastly, I would like to give a sincere thank you to the rest of my friends and family who were always present with open ears to listen when I simply needed someone to talk to.

TABLE OF CONTENTS

LIST OF TABLES

LIST OF FIGURES

ABSTRACT

The research presented in this thesis focused on the derivation of experimental fragility curves for windborne debris (WBD) impact risk assessment of building envelope components (BECs) with ductile behavior (in particular, aluminum storm panels) within the performance-based hurricane engineering (PBHE) framework. Using a pneumatic wind cannon, rod-type WBDs were fired at aluminum storm panels to represent real-life WBD impact hazard. The experimental data from testing were used to derive the probability of failure relative to specific damage measures (*DM*s) versus its corresponding interaction parameter (*IP*). These experimentally derived probabilities were compared with results that are available in the literature and were obtained from finite element (FE) analyses.

It was found that: (1) the impact kinetic energy of rod-type missiles is a sufficient *IP* for BECs with ductile behavior subjected to WBD impact; (2) the performance of aluminum storm panels (particularly in terms of probability of penetration) is strongly dependent on the details of the panels' installation; (3) the numerical results available in the literature regarding the fragility curves of BECs with ductile behavior are qualitatively representative of the behavior of aluminum storm panels subject to WBD impact; and (4) careful modeling of the actual mechanical behavior of the panel's boundary conditions is necessary for accurate numerical evaluation of the fragility curves of BECs with ductile behavior. It is noteworthy that accurate fragility curves are essential in the development of a general probabilistic performance-based engineering framework for mitigation of WBD impact hazard.

1. INTRODUCTION

1.1. Motivation

With massive hurricanes (e.g., Katrina in Louisiana in 2005), devastating tornados (e.g., Alabama's in 2011), and extreme earthquakes and tsunamis (e.g., Chile's in 2010), the threat to society that natural disasters propose is one that has gained worldwide attention. In the United States, specifically in the southeast region, hurricanes are the major concern. These strong natural forces have repeatedly caused severe damage to structural and infrastructural systems. Even tropical storms (i.e., storms that do not gain the necessary strengths to be classified as hurricanes) have led to immense structural damage, sometimes even causing the loss of life. Therefore, it has become more important over the years for engineers to be able to design structures that are able to adequately accommodate extreme loading conditions, such as those that result from hurricane events. In the last few decades, significant advances have been achieved in risk assessment and mitigation for structures subjected to hurricane threat. However, with constant ongoing advancements in building materials, it is essential that the advancement of structural reliability analysis and the development of performance-based engineering (PBE) techniques follow the fast technological pace. Such techniques allow for the consideration of uncertainties in engineering problems, and can be used for the calibration of design codes (Ghobarah 2001, Bertero and Vitelmo 2002, Cromartin 2004, Lebrun and Dutfov 2009). Amongst all of the tools being developed in probabilistic performance-based engineering, fragility curves are probably the most significant. They are the cumulative distribution functions (CDFs) of the structural capacity relative to a

specific limit-state, usually corresponding to a physical damage state for the structural system under consideration (Mackie and Stojadinovic 2004).

This research focused on the evaluation of experimental fragility curves that represent the damage states for aluminum storm panels subjected to windborne debris (WBD) impact loading. These fragility curves were obtained based on results gained from experimental testing using a wind cannon to replicate hurricane force winds. The WBD considered in this study were 2" x 4" dimensioned lumber missiles, which were fired at the aluminum storm panel using testing procedures that account for inherent uncertainties in both the aluminum storm panels and in the loading, produced by WBD impact. These fragility curves are an essential component of the performance-based framework for WBD hazard mitigation.

1.2. Performance-Based Engineering in Hurricane Engineering

Intense natural events (e.g., hurricanes) are often the cause of extreme structural damage as well as loss of human life. Thus, it is critical for engineers to design structures that accommodate the loading conditions accompanying these natural events. Within the past decade, significant advances in risk assessment and mitigation for structures subjected to hurricane hazards have been achieved (Holmes 2008). Structural reliability analysis and the development of probabilistic performance-based engineering techniques have been the two key elements to the growth and advances in this research and practice field. Modern structural reliability analysis techniques allow for rigorous consideration of uncertainties in engineering designs and are used to help develop more rational design codes (Nowak 1999, Kwon et al. 2010). Probabilistic performance-based methods are extensively developed in the field of earthquake engineering (Cornell and Krawinkler

2000, Porter 2003). Similar methodologies, which are based on a performance-based engineering approach, are currently being advanced in other civil engineering subfields including wind engineering, fire engineering, and blast engineering (Augusti and Ciampoli 2006, Li and Ellingwood 2006)

The PBE approach aims to achieve target levels of performance for a structural system instead of using a regulatory approach, which attempts to prescribe common design solutions for an entire spectrum of problems, based on general equations and calibrated coefficients that are anticipated to sufficiently satisfy assumed levels of performance. The integral goal of the PBE approach is to assure that the probability over the entire life that a structure exceeds any limit state (e.g., structure failure, member buckling, extreme deformation and displacement, occupant discomfort) is sufficiently small (Bertero and Vitelmo 2002). In this approach, the response of a structure is defined by engineering demand parameters (*EDP*s) (e.g., maximum deformation, maximum displacement, maximum force applied on a member) and is evaluated with respect to varying levels of intensity measures (*IM*s). In earthquake engineering, several scalar (e.g., peak ground acceleration, first-mode spectral acceleration) and vector *IM*s have been identified and employed (Bertero and Vitelmo 2002, Luco and Cornell 2007). In performance-based engineering applied to wind and hurricane engineering, there is a need to introduce a new set of parameters (referred to as interaction parameters (*IP*)) in order to describe probabilistically the interaction between structural properties and environmental loading, as well as their effects on structural response. In this research, which considers hurricane engineering, the *EDP*s are considered as a function of *IP*s rather than *IM*s, consistently with the performance-based engineering approach applied to

hurricane engineering proposed in Barbato et al. (2013). In this approach, physical quantities related to mean wind speed are good candidates for use as efficient and sufficient *IP*s (Barbato et al. 2013).

The performance is determined by comparing the structural response to appropriate *DM*s, which are used to define physical states of damage (Kwon et al. 2010). The PBE methodology provides an estimate of structural risk in terms of the probability of exceeding a given value of a decision variable (*DV*), which corresponds to a specified level of performance (Der Kiureghian and Liu 1986, Ghobarah 2001, Barbato et al. 2011, 2013). A *DV* is a measurable quantity that describes the cost and/or benefit for the owner, the users, and/or the society resulting from the structure under consideration. To guide the rational selection of a final design, *DV*s for several design options can be compared.

The explicit consideration of uncertainties is the critical feature of probabilistic PBE methods. Uncertainties can be categorized into two different types, i.e., aleatory uncertainties and epistemic uncertainties. Aleatory uncertainties are due to natural variability of physical, geometrical, and mechanical properties, whereas epistemic uncertainties are due to lack of knowledge, imprecise modeling, and limited statistical information (Der Kiureghian 1996, Lupoi et al. 2006). Inherent randomness is fundamentally irreducible since it is an inevitability of nature. In contrast, implementing more accurate and realistic models can reduce epistemic uncertainties. Since the effects of a hurricane on the built and natural environment are characterized by significant uncertainties and cannot be predicted using only deterministic models, there is a great need to develop a probabilistic PBE methodology in the field of hurricane engineering.

One of the crucial research needs in performance-based hurricane engineering (PBHE) is the development of fragility curves for structural and non-structural components of buildings and built structures. It has been shown that most of hurricane's damage is connected to the breach of building envelope components (Holmes 2008). A building's envelope is usually defined as the system of non-structural components (e.g., non-load-bearing walls, windows, doors, roofing) that separate the building from the exterior environment. When these elements are impaired, the building's structure becomes more susceptible to damage such as internal wind pressure and water penetration from the extreme natural conditions (Holmes 2008). In hurricane prone regions, property owners use many different types of moveable reinforcement (e.g., plywood, aluminum storm panels, various types of hurricane shutters) in order to protect their buildings from envelope damage. This thesis focused on the use of aluminum storm panels for the protection of residential constructions.

1.3. Objectives and Scope

This thesis had the following four main objectives: (1) to determine an appropriate *IP* in regards to WBD impact upon a ductile protective material (e.g., aluminum storm panels); (2) to evaluate the performance of different installation options (corresponding to different boundary conditions); (3) to develop experimental fragility curves representing the probabilistic resistance of aluminum storm panels subjected to WBD impact by accounting for all pertinent sources of uncertainty; and (4) to compare these experimental fragility curves with numerical fragility curves that are available in the literature for the same aluminum storm panels, and that were obtained through finite element (FE) analysis. While the scope of this research is limited to experimentally

generated fragility curves for ductile building envelope components (BECs), the results of this study are crucial for the development of a PBE methodology for the mitigation of WBD impact in hurricane and tornado prone regions.

1.4. Thesis Outline

Chapter 2 of this thesis presents a literature review on probabilistic PBE methods with particular focus on a recently developed PBHE framework. Chapter 2 also discusses existing research pertaining to WBD impact on BECs such as windows and window protection systems.

Chapter 3 presents the experimental equipment and settings, including the wind cannon and its construction, the target frame built for impact testing, and the velocity and deflections measurement systems. This chapter also examines ASTM specifications and safety procedures, which were followed during the experimental testing.

Chapter 4 discusses the results obtained from the experiments, including the experimental fragility data obtained and their comparison with FE-based fragility curves for ductile BECs, which are available in the literature.

Chapter 5 presents the conclusions of this study, makes recommendations for implementation of the results presented, and provides suggestions for future research.

2. LITERATURE REVIEW

2.1. Probabilistic and Reliability-Based Methods in Structural Engineering

Modern design approaches (e.g., Load Resistant Factor Design) rely on probabilistic and reliability-based methods. However, most of the current design codes are based on approaches that are prescriptive in nature and not suitable to satisfy explicitly specified levels of performance (Nowak 1999, Kwon et al. 2010).

Application of probabilistic approaches to direct assessment of WBD risk is relatively recent. Twisdale et al. (1996) developed and early model that assesses the risk of failure in glazing components due to WBD impact. A simplified version of this model is employed by the HAZUS software (FEMA 2013) to predict the risk of damage to a glazing element during a given period of time, T, during an extreme hurricane event (Holmes 2008). The probability of damage, P_D, is given by:

$$P_D = 1 - \exp\{-N \cdot A \cdot T \cdot [1 - F_{\xi}(\xi_D)]\} \quad (1)$$

where N = average number of impacts per unit time and unit surface area, A = surface area of the glazing components, $F_{\xi}(\xi_D)$ = CDF of kinetic energy or linear momentum, and ξ_D = kinetic energy or linear momentum beyond which the glazing component is damaged. While this approach represents a significant advancement towards PBE in relation to ordinary prescriptive design codes, it continues to neglect important sources of uncertainty, such as the variability of the damage threshold; thus, it presents serious limitations when designing for structures that are subject to WBD hazard and other hurricane hazardous conditions.

Li and Ellingwood (2006) proposed an analysis framework based on the use of first-order reliability methods. These methods were used to probabilistically describe the performance of building components. To consider the uncertainty in wind speed modeling, three different models were used in the analysis, allowing for comparisons of the final results. Each model used a Weibull distribution with different site-specific distribution parameters to describe the wind speed. Fragility curves for roof and cladding elements were generated by conducting first order reliability analyses of controlling limit state functions at increasing levels of the wind intensity described by the 3-second gust speeds at 33 feet above the ground in exposure category C (ASCE 2006). These fragility curves proved to fit lognormal distributions with low sampling errors. By convolving the fragility models with wind speed models, the probability of failure of a specific component, P_f, was obtained as:

$$P_f = \int_0^\infty F_R(v) \cdot f_v(v) \cdot dv \tag{2}$$

where $F_R(v)$ = structural fragility, and $f_v(v)$ = probability density function (PDF) of the hurricane wind speed, v. This approach represented an important step forward in the development of a PBE methodology for hurricane engineering and WBD hazard mitigation.

2.2. Performance-Based Engineering (PBE) Approaches

PBE is a general methodology that (1) defines the performance objectives for structural systems during their design life, (2) provides criteria and procedures for verifying the achievement of the performance objectives, and (3) offers appropriate

methodologies to improve the design of structural systems. In the past two decades, substantial research efforts have been devoted to the development of PBE in earthquake engineering, leading to the performance-based earthquake-engineering (PBEE) framework (Bertero and Vitelmo 2002). Currently, the civil engineering community is showing interest in the extension of PBE to other subfields of structural engineering, including fire engineering, blast engineering, wind engineering, and hurricane engineering (Bertero and Vitelmo 2002, Comartin 2004, Aktan et al. 2006, Barbato et al. 2011).

The major innovation of a PBE approach is the capability of overcoming some of the limitations of prescriptive design approaches. Evaluation of the relative effectiveness with respect to a given performance requirement of multiple proposed designs, all of which are acceptable based on code prescriptions, is difficult if not entirely impossible. In addition, the prescriptive code requirements present a hold on design innovation and cannot be directly applied to the design of structures for which there is no previous knowledge of the existing conditions (Petrini 2009). Thus, applying prescriptive building codes, design standards, and mitigation techniques to all structures regardless of the existing conditions, the conditions forecasted, and location's relative frequency of hazard events, does not always pan out to be the correct solution (Augusti and Ciampoli 2008).

The use of PBE methodologies is widely regarded as the most rational approach for structural design considering risk due to natural phenomena (Augusti and Ciampoli 2008). When using the PBE methodology, the aim is to achieve specified levels of performance for structural designs, rather than designing a structure to withstand prescribed loading conditions. A design is acceptable if the probability that it does not

satisfy a specified limit state is sufficiently low. This criterion removes many of the restrictions of a prescriptive approach and allows engineers to identify an optimal structural design among a set of many possible designs for a given problem (Comartin 2004, Aktan et al. 2006). These methods also allow for the explicit consideration of uncertainties in structural loading resulting from highly unpredictable natural phenomena, such as earthquakes, hurricanes, and uncertainties in structural capacity emanating from variability in mechanical and geometrical properties (Lupoi et al. 2006). Due to these considerations, several modern seismic design guidelines have adopted PBE methods (FEMA 1997, ATC 2005).

The Pacific Earthquake Engineering Research (PEER) Center PBEE framework is a widely accepted example of PBE methodology. The PEER method aims to evaluate performance at both the component and system level in terms of *DV*s (e.g., structural response, repair costs, deaths, downtime after an earthquake) using a series of independent analysis phases, each describing probabilistically four different sets of quantities (e.g., *IM*, *EDP*, *DM*, *DV*) that are needed to fully describe the design problem. In addition, the PEER PBEE methodology rigorously accounts for uncertainties affecting each phase of the analysis, such as component fragility and ground motion variability (Porter 2003). In this methodology, the structural performance is evaluated by estimating the probability that specific levels of *DV*s will be exceeded for a specific structure subjected to seismic hazard. The final results of this methodology are the probability distributions of the potential loss to stakeholders of the structure in question. Available literature has shown that the use of PBEE methods can lead to more accurate loss

estimation and more efficient design for structures subject to seismic excitation (Comartin 2004, Aktan et al. 2006).

2.2.1. Performance-Based Hurricane Engineering (PBHE) Framework

Barbato et al. (2013) proposed an extension of the PBE methodology to hurricane engineering. This extension is referred to as PBHE framework and accounts for the different sources of hazard that are related to hurricane landfalls in hurricane prone areas, i.e., wind pressure, flooding, WBD impact, and rainfall. The PBHE framework accounts for the uncertainties related to the environment (i.e., the region not affected by the presence of the structure), the structure, and the exchange zone (i.e., the region in which natural actions interact with the structure). The PBHE framework is based on the total probability theorem (Ang and Tang 1975) and disaggregates the performance assessment procedure for structures subject to hurricane hazard into elementary phases, which are carried out in sequence. An important feature of the proposed procedure is the qualitative independence of each phase from the others (i.e., the choice of the parameters that are characteristic for a given phase is independent from the parameters adopted in the previous phases).

The structural risk within the PBHE framework can be defined in terms of a given *DV* as follows:

$$G(DV) = \int\int\int\int\int G(DV \mid DM) \cdot f(DM \mid EDP) \cdot f(EDP \mid IM, IP, SP) \cdot f(IP \mid IM, SP) \cdot f(IM) \cdot f(SP) \cdot dDM \cdot dEDP \cdot dIP \cdot dIM \cdot dSP \quad (3)$$

in which $G(\cdot)$ = complementary cumulative distribution function, $G(\cdot|\cdot)$ = conditional complementary cumulative distribution function, $f(\cdot)$ = probability density function, $f(\cdot|\cdot)$ = conditional probability density function, *DM* = damage measure, *EDP* = engineering

demand parameter (i.e., a parameter describing the structural response for the performance evaluation), *IM* = vector of intensity measures, *SP* = vector of structural parameters (i.e., the parameters describing the relevant properties of the structural system and non-environmental actions), and *IP* = vector of interaction parameters (i.e., the parameters describing the interaction phenomena between the environment and the structure). Note that in Equation (3), *IM* and *SP* are assumed as uncorrelated and independent of *IP*, while *IP* is dependent on both *IM* and *SP* (Barbato et al. 2013). The risk assessment procedure is disaggregated into the following six separate tasks: (1) hazard analysis, (2) structural characterization, (3) interaction analysis, (4) structural analysis, (5) damage analysis, and (6) loss analysis (see Figure 1).

Hazard analysis, structural analysis, damage analysis, and loss analysis were described in detail by Moehle et al. (2006) as part of the PEER PBEE framework. Structural characterization and interaction analysis were introduced for the first time as part of the performance-based wind engineering framework in order to model the effects on the structural response of the interaction between the structural system and the environment (e.g., aerodynamic effects) (Ciampoli et al. 2009). In particular, the probabilistic hazard analysis phase requires the identification of the (joint) probability density function $f(IM)$. The *IM* within this task should be chosen as strictly independent on the investigated structure. Therefore, while engineers hold the duty of clarifying what information is needed, the probabilistic information regarding the *IM* should be provided by meteorologists, climatologists, and other experts in atmospheric sciences (Barbato et al. 2013).

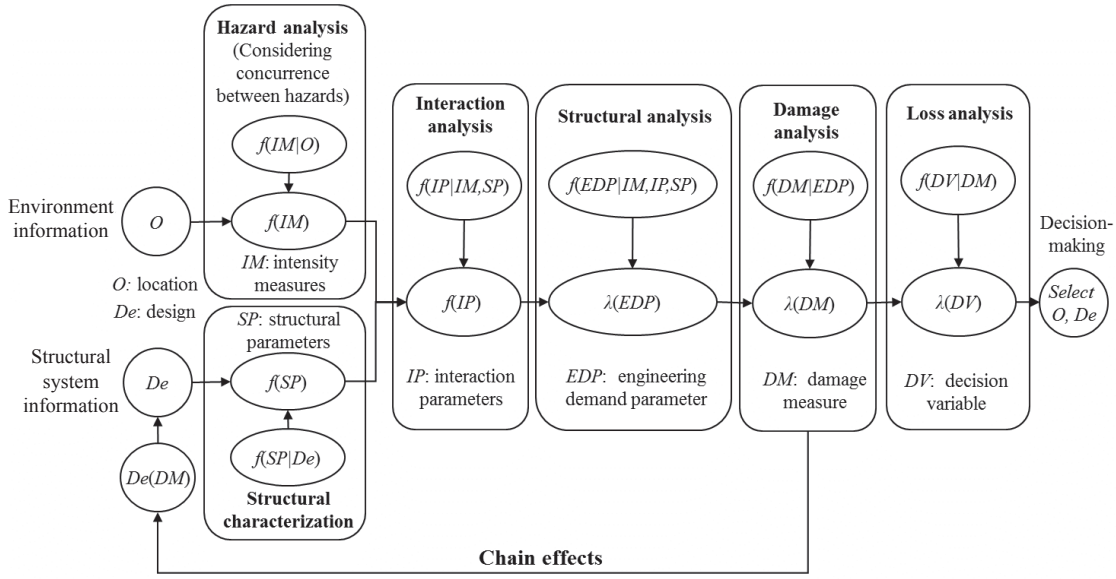

Figure 1: Probabilistic analysis components in the PBHE framework (adapted from Barbato et al. 2013)

2.2.2. Identification of *IP*s

In PBEE, *IM*s are used to describe the uncertainties in the seismic loading conditions and the seismic hazards corresponding to the specific location of a structure. These *IM*s must satisfy the conditions of sufficiency and efficiency. An *IM* is said to be sufficient when it renders an *EDP* independent of the earthquake's magnitude and site to source distance. An *IM* is said to be efficient when its use produces a small variance in the *EDP* (Luco and Cornell 2007).

In PBHE, *EDP*s are considered as a function of an *IP* rather than an *IM*, such as the case in PBEE. Thus, when referencing the parameters that describe the interaction phenomena between the environment and the structure, the vector *IP* will be used. Numerous studies (e.g., Baker and Cornell 2005, Vamvatsikos and Cornell 2005, Luco and Cornell 2007, and Baker and Cornell 2008) have addressed the problem of selecting

sufficient and efficient *IM*s for different structural response quantities in PBEE. In these studies, it was found that no single *IM* is sufficient and efficient for all types of structures. Thus, the determination of a sufficient and efficient scalar or vector *IP* for a specific response quantity of a specific structure (or structural typology) subjected to hurricane hazard is an integral part of the PBHE (Barbato et al. 2013).

2.2.3. Fragility Analysis

A fragility analysis is the component of a probabilistic PBE approach which provides the probabilistic representation of the structural capacity of a structure or of a structural component with respect to a specific limit state in the form of fragility curves, i.e., CDFs of *DM*s conditional to specific values of the corresponding *EDP*s (Porter 2003). One of the major elements of fragility analysis is the identification of the pertinent limit states for a specified structural component and its corresponding elements. It is noted here that the term "fragility curve" is used in the literature for *DM-EDP* relations (Beck et al. 2002), *DM-IM* relations (in PBEE, Lupoi et al. 2006), and *DM-IP* relations (in PBHE, Barbato et al. 2013).

Fragility functions are often assumed to follow lognormal distributions (Beck et al. 2002). Under this assumption, the *EDP* value that corresponds to a given probability of structural damage, *p,* can be determined from a lognormal CDF as:

$$x_p = x_m \cdot \exp[\beta \cdot \Phi^{-1}(p)] \tag{4}$$

in which x_p = value of the *EDP* corresponding to the probability of damage p, x_m = mean of the distribution, β = log standard deviation of the distribution, and $\Phi^{-1}(p)$ = inverse of the standard normal CDF computed at probability p.

Significant research efforts have been devoted to the study of fragility analysis in earthquake engineering (e.g., Porter et al. 2001, Beck et al. 2002, Porter et al. 2002, Mackie and Stojadinovic 2004, Lupoi et al. 2006). Porter et al. (2001) observed that fragility functions can be obtained from either empirical or theoretical data. In their study, fragility functions for structural and nonstructural components of a welded steel moment frame building subject to seismic excitation were derived using both empirically and theoretically obtained data available in the literature describing the structural components of interest. In the study by Beck et al. (2002), fragility functions for reinforced concrete beam-columns subject to seismic excitation, which corresponded to a number of damage states ranging from light damage to collapse, were derived. The fragility functions were derived using existing empirical data, which regarded the failure of the specified structural components. From the fragility functions, fragility curves where then generated with respect to the displacement damage index, *DDI*, defined as the structural damage resulting only from member displacements (i.e., curvatures) during seismic loading. The *DDI* was defined as:

$$DDI = \frac{\phi_m - \phi_r}{\phi_u - \phi_r} \tag{5}$$

where ϕ_m = maximum curvature achieved by the beam-column under loading, ϕ_r = recoverable curvature after unloading of the beam-column, and ϕ_u = nominal ultimate curvature capacity of the beam-column. Figure 2 shows that, as the magnitude of *EDP* increases, the damage states become more severe and the probability of failure increases.

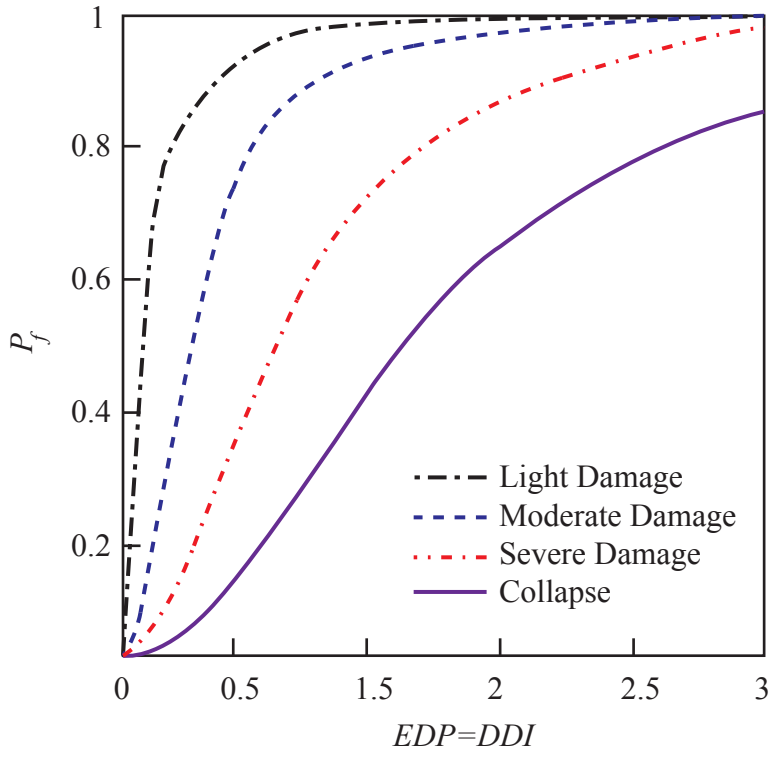

Figure 2: Examples of fragility curves relative to multiple damage states for concrete beam-columns subject to seismic excitation (adapted from Beck et al. 2002).

2.3. Existing Literature on WDB Impact Research

Significant research efforts have been dedicated to experimental testing and numerical simulations of the structural response and performance of different types of BECs subjected to WBD impact. This section of the thesis provides a brief literature review of recent research results on WBD impact.

2.3.1. Sources of WBD

WBD can be generated from numerous sources. In residential constructions, the most common WBD comes from roof cladding, roof and wall framing elements, vegetation, road signs and signal components, as well as a variety of items usually found

in private yards, such as garbage cans, mailboxes, and home decorations (Masters et al. 2009, Fernandez et al. 2010). Approximately half of all WBD causing damage is generated from roof cladding elements, with one-tenth being generated from roof framing elements, and another tenth generating from other roof attachments (Holmes 2008). WBD from residential buildings usually begins with roofing materials on neighboring buildings, which causes a "chain reaction" of damage: WBD impact nearby constructions, damaging them and producing additional WDB that can produce further damage on other adjacent buildings (Holmes 2008). WBD usually originates at higher elevations, such as the highest roofline, and this WBD has the potential to cause more damage compared to WBD that is generated at lower elevation. This higher damage potential is due to the longer flight trajectories, which allow the WBD to achieve higher velocities (Holmes 2008).

The trajectory of WBD is key when trying to understand how WBD impacts affect and occur on built structures. Three different types of WBD can be identified in terms of typical trajectories: (1) compact-type debris, (2) rod-type debris, and (3) sheet-type debris (Willis et al. 2002, see Figure 3).

Compact-type WBD are small, pebble like debris with no capability of reaching aerodynamic lift (see Figure 3(a)). Rod-type debris are long, slender lumber and tree branch-type projectiles that may achieve aerodynamic lift, but only at small levels (see Figure 3(b)). Sheet-type debris have wide and flat shapes and are capable of reaching high levels of aerodynamic lift, giving this debris the ability to travel longer distances while airborne (see Figure 3(c)).

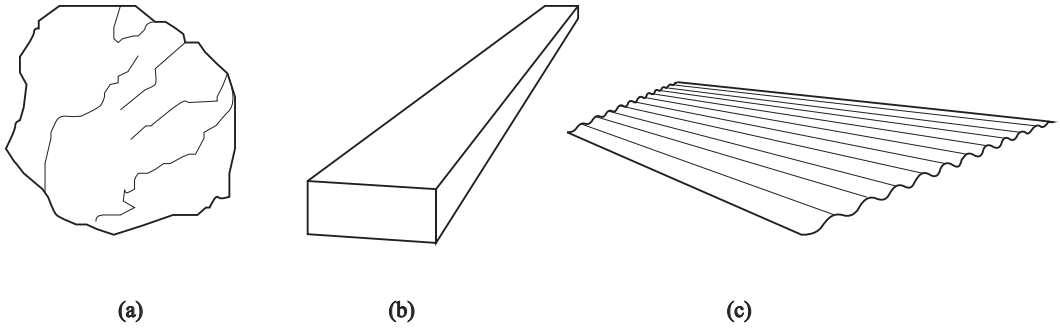

Figure 3: Types of WBD: (a) compact-type, (b) rod-type, and (c) sheet-type WBD.

Figure 4 illustrates typical trajectories for these three categories of WBD. The focus of this thesis is to investigate the effects of 2" x 4" dimensioned lumber (i.e., rod-type debris).

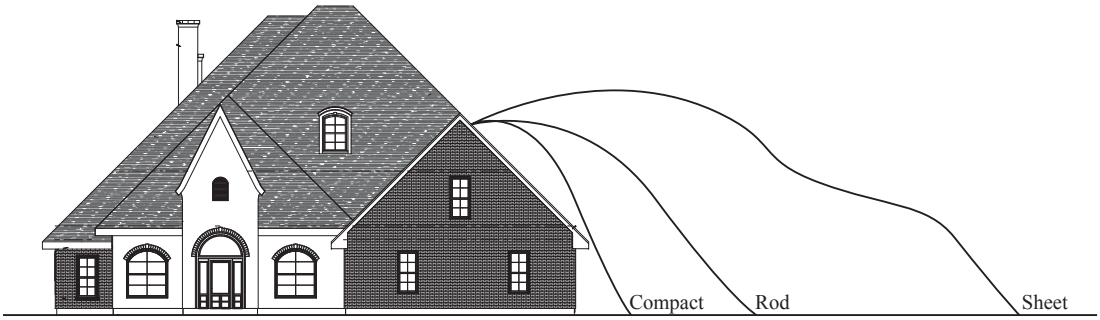

Figure 4: Typical trajectories for WBD

Willis et al. (2002) determined mathematical relationships describing the liftoff wind speed by considering the balance of the forces (i.e., gravitation and aerodynamic forces) applied to WBD during hurricane events. For the rod-type WBD, the threshold wind field velocity that leads to liftoff and flight, u_{rod}, is given by

$$u_{rod} = \sqrt{\frac{\pi}{2} \cdot (\rho_m / \rho_a) \cdot (I / C_F) \cdot d \cdot g} \qquad (6)$$

where ρ_m = density of the material of the missile, ρ_a = density of the air, I = fixture strength integrity (i.e., the measure of the wind force required to displace items from the original structure), C_F = aerodynamic force coefficient, d = effective diameter of the missile (i.e., the diagonal dimension of the 2" x 4" lumber missile), and g = gravitational acceleration constant. Using Equation (6), it was estimated that wind speeds in excess of 72 mph would likely cause a typical 2" x 4" dimensioned lumber missile with a length of 8 feet to achieve liftoff (Willis et al. 2002).

Several studies analyzed the trajectories of WBD using wind tunnels and full-scale tests (Lin et al. 2006, 2007). It was found that the maximum horizontal velocities achieved by the three types of WBD can be described by a function of the WBD horizontal flight distance, mass, and drag properties. For rod-type debris (e.g., 2" x 4" dimensioned lumber projectiles), the ratio of horizontal missile speed, u_m, to wind velocity, U, can be approximated as:

$$\frac{u_m}{U} \approx 1 - e^{-\sqrt{0.058x}} \tag{7}$$

where x = horizontal displacement of the rod-type debris (Lin et al. 2006, 2007). Figure 5 plots the functional relation given by Equation (7).

In Figure 5, it is observed that the largest acceleration of rod-type WBD occurs in the first 5 to 10 meters of flight, during which the WBD can reach approximately 30-50% of the wind field velocity.

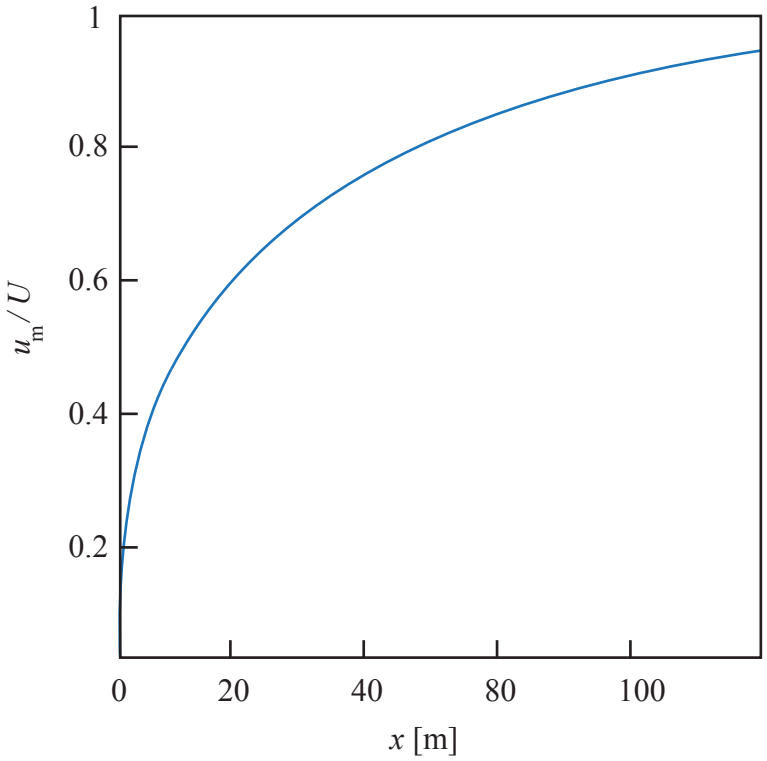

Figure 5: Ratio of horizontal missile speed to wind field velocity for rod-type WBD as a function of flight distance (adapted from Lin et al. 2007).

2.3.2. WBD Impact on BECs with Brittle Behavior

The consequence from WBD impacting window glass and its vulnerability has provided many researchers with motivation to study WBD. It is noted here that almost all studies conducted regarding brittle behaving BECs have identified linear momentum, LM_m, as a suitable *IP* to be used for fragility analysis. The National Association of Home Builders (NAHB) research center conducted a study where annealed glass window samples of different sizes and thicknesses were subjected to 4.600lb (20.466N) 2" x 4" rod-type WBD impacts at fluctuating levels of missile impact linear momentum (NAHB 2002). These missiles were simulating WBD generated from roof framing elements in the event of a hurricane. Several window specimens were tested at multiple levels of LM_m in

order to assess the fragility of the annealed glass specimens. From these tests, the probability of failure was recorded as the ratio of the number of windows that broke on missile impact versus the total number of trials *n* at each level of LM_m (NAHB 2002). The study concluded that, for a 61cm x 61cm specimen with a 3.970mm thickness, window failure was almost certain at $LM_m \geq 7.198\text{kg}\cdot\text{m/s}$.

Masters et al. (2009) used laboratory experiments to assess the vulnerability of double-strength annealed glass subject to impact by different types of debris with different impact orientations. The glass specimen tested was once again 61cm x 61cm, with a thickness of 3.180mm. Other WBD types commonly found in post-storm surveys, including rod-type wooden dowel missiles with diameters of 2.540cm and 5.080cm, and masses equal to 200g, were also part of the testing. These missiles were intended to replicate tree branches and limbs, which tend to become WBD during hurricanes. The result of this testing was a "Vulnerability Curve", which is a fragility curve using PBE terminology. In order to obtain this vulnerability curve, $N = 20$ window specimens were tested at multiple levels of LM_m for a case corresponding to head-on impacts using the two types of dowels. Through these tests, it was observed that unprotected glass specimens impacted by lightweight rod-type WBD present almost a 100% failure probability for impact linear momentum values as low as $LM_m \geq 4\text{kg}\cdot\text{m/s}$ (Masters et al. 2009). The differences between the LM_m levels that correspond to almost sure failure of brittle glass BEC specimens, as obtained in Masters et al. (2009) and NAHB (2002), suggest that the type of WBD impacting the brittle BECs significantly influence their fragilities.

The fragility curves obtained in Masters et al. (2009) and NAHB (2002) are among the first probabilistic descriptions of BEC performance under WBD impact. They showed that brittle BECs are extremely vulnerable to failure and damage from rod-type WBD impacts, regardless of the level of LM_m. Masters et al. (2009) and NAHB (2002) also suggested that WBD impact protection systems are absolutely essential to ensure acceptable levels of performance by structures located in hurricane prone areas. The most common WBD impact protection systems have ductile behavior.

2.3.3. WBD Impact on BECs with Ductile Behavior

Research available in literature regarding the performance of BECs with ductile behavior subjected to WBD is very scarce and relatively recent. In Borges et al. (2009), the performance of aluminum and steel storm shutters subject to WBD impacts, based on the Miami Dade County test protocols, were studied through numerical analysis. A deterministic FE model was used to simulate WBD impact. The model constructed considered storm shutters that were mounted on a fixed-rail system along two sides and left unconstrained along the other two sides. The following results were obtained: (1) material failure was not observed in any trials due to the high level of flexibility in the model and the impact energy dissipation through panel deformation; (2) the highest level of damage was recorded in impacts occurring along the unrestrained outer boundaries of the panels, as well as in the instances when the missile passed the panel and entered into unrestricted contact with the protected BEC with brittle behavior; and (3) the applied boundary conditions and the geometry of the panel significantly affected the response of the panel in terms of deformations (Borges et al. 2009).

Fernandez et al. (2010) also addressed the performance of aluminum storm panels subject to WBD impact by conducting experimental tests. Numerous sources of WBD and their impacts were considered, with particular focus on clay roof tiles and 9-lb 2" x 4" dimensioned lumber missiles. The impact velocity of the WBD was at a constant 15.250m/s for all trials. Similar to Borges et al. (2009), the boundary conditions consisted of a fixed-rail system mounted along two sides, with the other two sides left unconstrained. The conclusions identified in the above study were: (1) WBD impacts near the panels' corners and track boundary conditions can damage the panels in a "pull-out" or "push-through" pattern (i.e., the damage at the mounting track affects the panels integrity), (2) debris of the same weight and impact velocity but of different shapes and impact orientations can cause different levels of damage when impacting storm panels, and (3) commonly accepted 2" x 4" dimensioned lumber impact testing standards may be insufficient to ensure a target level of performance, since impact velocities are likely to exceed the value of 15.250 m/s used in the standard testing and missile types are not uniform during a design level hurricane event (Fernandez et al. 2010). These conclusions suggests that the current best practices do not account for the typical variability observed in WBD impact during hurricane events and, thus, an alternative and more accurate methodology is needed to ensure that performance of BECs and BEC protection systems meet a satisfactory performance criterion.

Herbin (2011) and Herbin and Barbato (2012) studied aluminum storm panels that were identical to those considered in the present study. Those studies presented a methodology for developing WBD impact fragility curves for BECs by using stochastic finite element models. These fragility curves provide the probabilistic description of the

impact resistance of BECs subject to an impact event described by an appropriate *IP*. It is noted here that, in Herbin (2011) and Herbin and Barbato (2012), the fragility curves were derived as *DM-IM* relationships, consistently with the PEER PBEE framework, since the PBHE framework was not yet formulated (Barbato et al. 2013). Thus, the quantities referred to as *IM*s in those studies coincide with the *IP*s considered in the present study. Monte Carlo simulations were used in combination with FE methodologies to propagate uncertainties in the BEC's model parameters and WBD impact location. Several fragility curves for aluminum storm panels subjected to WBD impact were derived for different damage measures. It was found that (1) the missile kinetic energy at impact is a sufficient *IP* for BECs with ductile behavior subjected to WBD impact, and (2) the performance of storm panels in terms of penetration of WBD is critically dependent on the details of the panel installation.

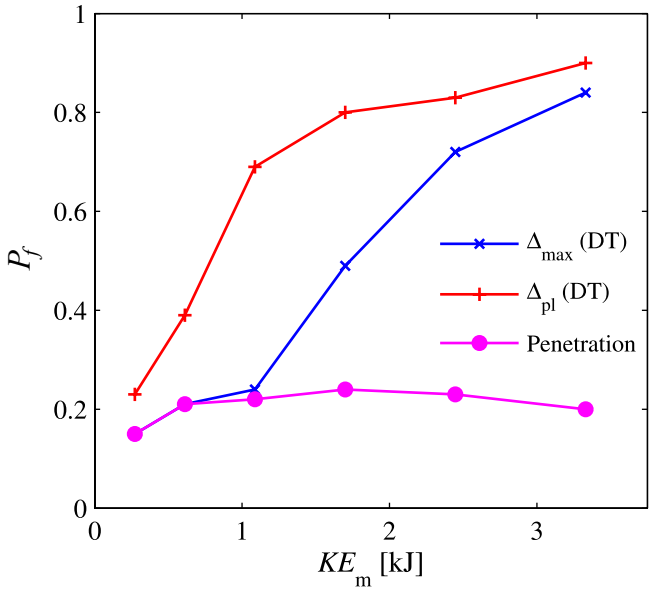

Figure 6: FE-based fragility curves for aluminum storm panels (adapted from Herbin and Barbato 2012)

Figure 6 plots the probability of failure relative to each limit state identified in Herbin and Barbato (2012) as a function of $IP = KE_m$. Each data point in Figure 6 is representative of 100 stochastic FE simulations at the corresponding *IP* level. Therefore, the probability of failure with respect to each *DM* is the number of total failures out of 100 total trials for each discrete KE_m level.

2.4. Experimental Facilities for Study of WBD Impact Hazard

Only few experimental facilities, often connected with University research centers, focus on WBD impact in the U.S. The following subsections identify select experimental facilities and the experiments conducted within those facilities, which are relevant to the research presented in this thesis.

2.4.1. Texas Tech Wind Science and Engineering Research Center

Texas Tech's Wind Science and Engineering Research Center is a research center focused on wind effects on structural systems. The equipment available within this research center includes a pneumatic cannon that is used for the purpose of analyzing hurricane and tornado force impact effects on BECs. The cannon uses a pneumatically actuated butterfly valve to release air pressure contained inside a 30-gallon pressure vessel to project an object against an intended target.

Extensive testing of the operations of the cannon was needed to derive the relationships between the desired shooting velocity and the charge pressure for several specified projectile types. These relationships were stored in an experimental notebook that can be used by the operators to find the charge pressure for the specific projectile and the desired missile velocity. Two analog velocity measurement systems accompany the

cannon, and provide the operator with accurate velocity measurements of the projectiles leaving the cannon. All of these devices are connected and/or are located near the operators cart.

One key property of Texas Tech's cannon is its mobility. The cannon can be adjusted vertically by a hydraulic scissor lift, and horizontally by a threaded rod that is powered by a small electric motor. Vertical and horizontal mobility allow the operators to easily adjust the cannon to fire at varying BEC locations. Based on ASTM specifications for impact testing, the BEC needs to be impacted at two different locations (i.e., at the center and at the corner near the boundary conditions)(ASTM 2006). Thus, the cannon mobility significantly simplifies the impact testing procedure.

Texas Tech has successfully conducted numerous experiments with the pneumatic cannon. However, all of the experiments focused on the response of brittle BECs impacted by WBD, with LM_m used as the *IP* (Levitan et al. 2009). The data collected is the probability of failure with respect to the varying levels of LM_m. Examples of BECs tested with the Texas Tech cannon are concrete-masonry unit block walls, red brick masonry walls, and annealed glass windowpanes. The tests were mainly intended to obtain a limit value for LM_m beyond which failure of each BEC is almost sure.

2.4.2. FIU International Hurricane Research Center

The Florida International University's International Hurricane Research Center is a research facility with equipment capable of simulating Category 5 hurricane force winds – the highest rating on the Saffir-Simpson Hurricane Wind Scale (Aly et al. 2011, 2012). In 2005, FIU's wind engineering team assembled their first prototype, which was a 2-fan mobile unit that could generate 120 mph winds with a water-injection system to

simulate horizontal rain during hurricane events. Due to increased demand for higher wind speeds, the research center designed and built the RenaissanceRe Wall of Wind (WOW). The WOW consists of 12 large-scale fans and is capable of performing controlled and repeatable full-scale testing in flows that replicate the same Category 5 level winds as Hurricane Katrina in 2005.

Among the experimental tests carried out using the WOW facility, a full-scale test was performed to evaluate wind-induced external and underneath pressure coefficients acting on loose concrete-pavers mounted on a building (Aly et al. 2012). The pressure coefficients at various locations on the roof paver system were evaluated for five different wind directions. The tests provided information regarding the worst-case scenarios in terms of wind direction and location of the pavers on the roof. To this date and to the best of the author's knowledge, there are no published studies at the WOW facility regarding fragility analysis of structural and non-structural building components.

2.5. Design Code Requirements for Mitigation of WBD Impact Hazard

The International Building Code (IBC 2012) requires that glazing elements on structures located in hurricane prone regions must be protected by an impact resistant covering (e.g., aluminum storm panels and shutters), or be impact resistance. The performance rating of these BECs must be assessed using ASTM E1996 and ASTM E1886 test standards. Glazing elements located less than 30 feet above grade must be tested using "large missiles" (i.e., 9-lb 2" x 4" dimensioned lumber missiles), as defined in ASTM E1996, for a range of typical WBD impact velocities during hurricanes, which are given as 9 to 30 m/s (20 to 70 mph) (ASTM E1886).

The testing procedure described in ASTM E1996 and ASTM E1886 requires to subject an impact resistant BEC to WBD impacts at prescribed locations on its surface and then to cyclical pressure loading, (i.e., cycling from positive to negative pressure) to simulate the conditions experienced by the BEC during a hurricane. The prescribed impact locations are the center and a corner of the BEC. ASTM standards do not supply explicit installation instructions for the BECs, which need to be installed according to the manufacturer's installation specifications.

Storm protection systems need to meet the minimum requirements set by the ASTM testing protocols and are noted in terms of maximum wind speed and importance of the facility in which they can be used. It is observed that the existing ASTM codes are prescriptive in nature, do not account for the uncertainty that accompanies extreme events such as hurricanes, and do not allow for direct performance considerations.

3. EXPERIMENTAL SETUP

3.1. Introduction

This thesis focuses on the construction of fragility curves of BECs with ductile behavior. These fragility curves are a fundamental ingredient of PBHE (Barbato et al. 2013). An important contribution of this research is the experimental identification of the appropriate *IP*s, *EDP*s, and *DM*s, which are needed for WBD impact assessment. The fragility curves are based on results obtained from firing WBD missiles at BECs using a pneumatic wind cannon. The proposed methodology is applied to the specific case of an aluminum storm panel, which is representative of BECs with ductile behavior, and is subject to WBD impact hazard of 2" x 4" dimensioned lumber missiles (i.e., 9-lb, 12-lb, & 15-lb). This chapter describes the experimental facility, equipment and settings used to derive the experimental fragility curves.

3.2. Experimental Equipment

The experimental campaign was performed using the LSU wind cannon, which is located at the Louisiana State University Blowout Prevention Facility in Baton Rouge, LA. The experimental equipment consists of: (1) a steel pneumatic cannon, (2) a velocity measurement system, (3) a support target frame, and (4) a deflection measurement system. The following subsections describe in more detail the equipment used to perform the experimental tests.

3.2.1. LSU Wind Cannon

The LSU wind cannon is a pneumatically actuated steel cannon with computer control that fires projectiles simulating WBD generated by hurricane force winds. This cannon exceeds ASTM E1866 and ASTM E1996 testing standards, provides accurate velocity measurements, and is characterized by high horizontal and vertical mobility. The prototype equipment was preliminarily designed in 2003 and after numerous design iterations and improvements, was completed in 2009.

LSU's wind cannon has the main function of shooting projectiles (e.g., 2" x 4" dimensioned lumber missiles and small steel balls), which simulate flying debris caused by hurricane force winds. The cannon itself consists of a 15-foot-long barrel with a 6" nominal diameter. Located above the barrel is a 30-gallon pressure vessel used to hold pressurized air, which provides the force needed to drive the projectile to the desired velocity. The amount of pressure contained within the vessel can be instantly released by a 6" pneumatic butterfly valve. This butterfly valve can be opened through a master air cylinder that is controlled by a four-way 110V AC solenoid valve. The solenoid-operating signal originates from the lockable control box, which is used as a safety precaution. The safety box includes a safety-keyed switch that stops the flow of energy so that the cannon cannot be fired accidentally. A mechanical winch attached to the base structure controls the vertical movement of the cannon, while the horizontal (side-to-side) movement of the cannon is controlled by a hand-operated crank. Figure 7 through Figure 10 show the components of the LSU wind cannon.

The LSU wind cannon presents the following two major advantages when compared to the Texas Tech wind cannon:

(1) The LSU's cannon houses a 6" barrel rather than a 4" barrel. A larger sized barrel allows for testing of specimens subjected to impact of numerous smaller projectiles at the same time (e.g., multiple small steel balls) and larger single projectiles (e.g., 2" x 6" lumber missile).

(2) The barrel of the LSU wind cannon is made of steel rather than PVC. By using a steel barrel, a higher safety is ensured for operators and bystanders, since the barrel cannot shatter under high pressures. In addition, higher pressures can be reached in the barrel, thus making possible to perform impact tests with higher velocities for wooden missiles or with heavier projectiles (e.g., steel pipes). Finally, the use of a steel barrel practically eliminates the need for the replacement of the barrel and, thus, reduces significantly the operating costs of the LSU wind cannon. It is noted here that, in the Texas Tech wind cannon, the PVC barrel must be replaced every 25 to 50 firings.

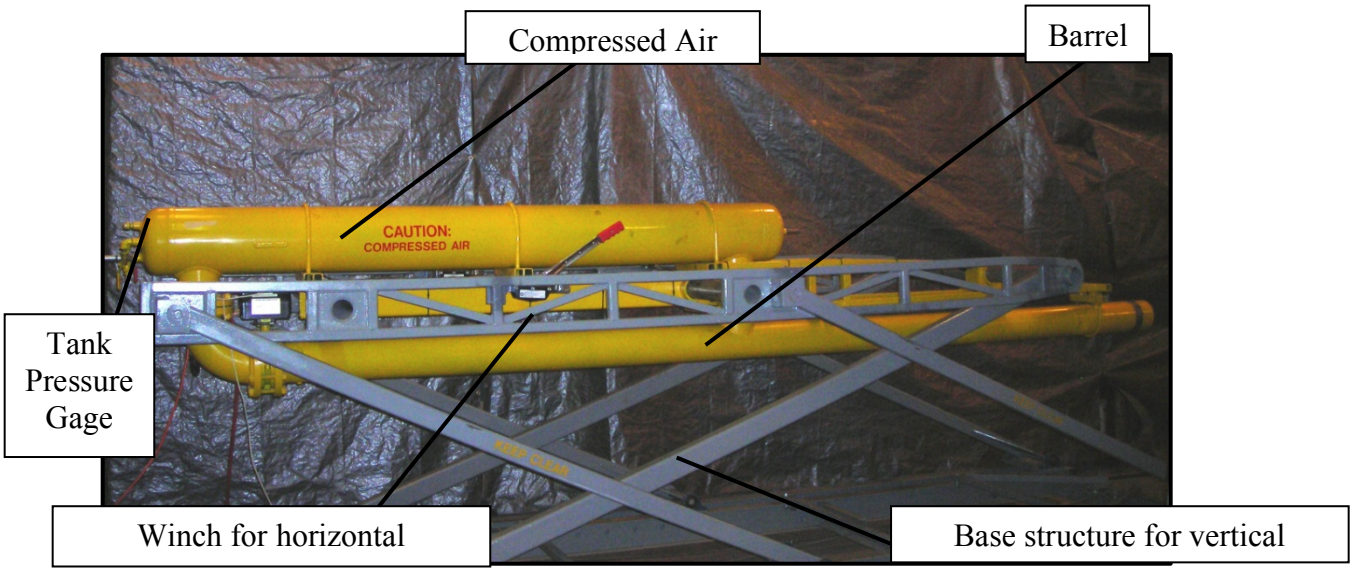

Figure 7: LSU wind cannon's main components

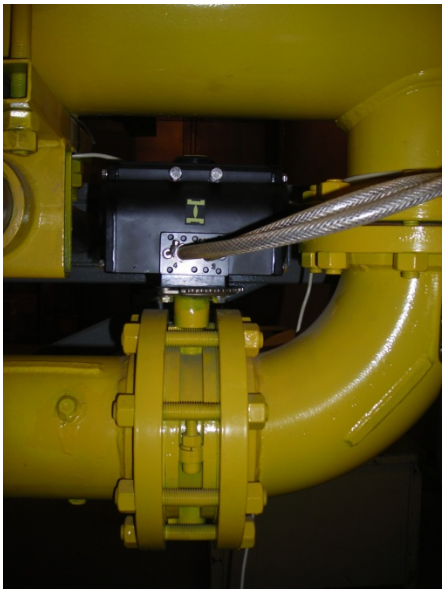

Figure 8: 6” butterfly valve of the LSU wind cannon

(a)

(b)

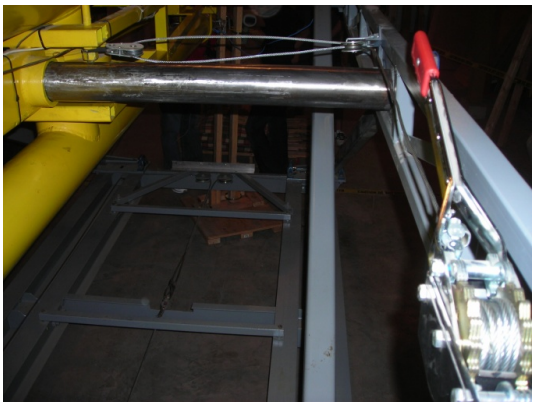

Figure 9: Horizontal mobility components of the LSU wind cannon:
(a) hand winch, and (b) pulley system

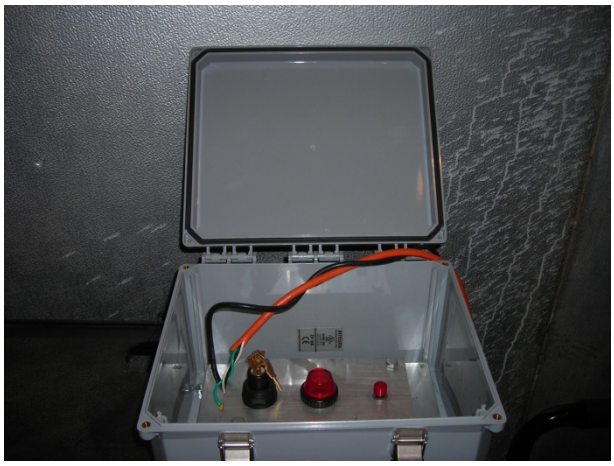

Figure 10: Firing Box

3.2.2. Velocity Measurement System

The velocity measurement system (VMS) for the missile velocity consists of a shooting chronograph with a dual sensor system to provide accurate projectile velocities that can be recorded using different units of measure. The technology used in chronographs is quite simple. The device houses two light sensors that are strategically placed at an accurately measured separation distance, *S*. As a projectile breaks the first sensor's plane, the sensor transmits a signal to the circuit board, which records the time when the first sensor's plane was broken, t_1. When the projectile breaks the second sensor's plane, another signal is sent to the circuit board, once again recording the time at which the second sensor's plane was broken, t_2. The difference between these two times is used to calculate the velocity of the projectile, *V*, as:

$$V = \frac{S}{t_2 - t_1} \tag{8}$$

The chronograph used with the LSU wind cannon is the Alpha Beta Master chronograph produced by *Shooting Crony*. The chronograph chosen far exceeds the

ASTM standard specifications required for hurricane WBD impact testing. This chronograph has a detachable LCD display to present the recorded velocity. The unit is able to store up to 1,000 readings, which can then be readily transferred to computer applications, such as Microsoft Excel, for post-processing of the data. The Alpha Beta Master chronograph is equipped with two small light diffusers to be placed above each sensor, assuring the best lighting conditions for each sensor. Since the open distance between the sensors and the unit was insufficient for safe firing, a larger diffuser was built to ensure appropriate lighting conditions were present for accurate velocity readings (see Figure 12).

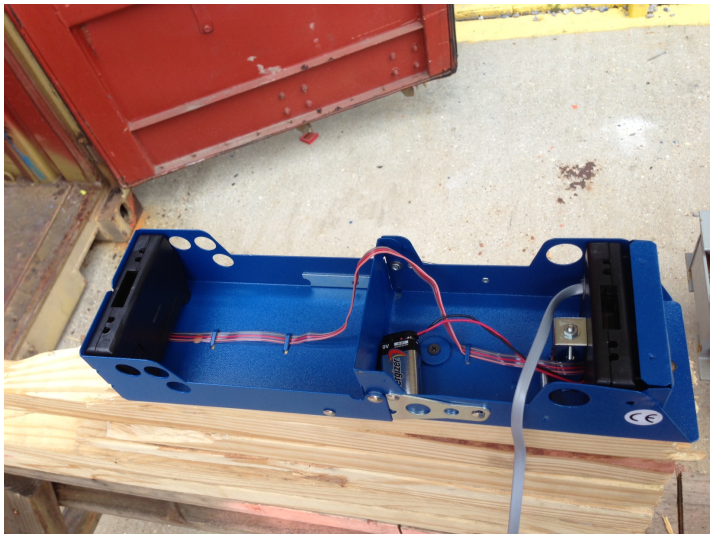

Figure 11: *Shooting Chrony* Alpha Beta Master chronograph

Figure 12: Large scale light diffuser for VMS

3.2.3. Derivation of Pressure-Velocity Curves for the LSU Wind Cannon

The use of the LSU wind cannon requires the derivation of pressure-velocity curves for the different projectiles to be used experimentally. These pressure-velocity relations are needed by the cannon's operator in order to set the pressure in the air tank that produces the desired velocity for the projectile with a specified accuracy. Due to the large number of variables affecting the projectile's velocity (e.g., air leaking around the sabot, inclination and positioning of the missile within the barrel), as well as the significant uncertainties affecting these variables, the pressure-velocity curves for a specific wind cannon need to be obtained experimentally for different types of missiles.

Three 2" x 4" missile types were considered: (1) 9-lb (corresponding to a mass of 4.08kg), (2) 12-lb (corresponding to a mass of 5.44kg), and (3) 15-lb (corresponding to a mass of 6.80kg). First, repeatability tests were performed. Each missile type was fired at the same value of pressure five times, conducting fifteen tests. After the repeatability tests demonstrated that both the VMS and the cannon were providing repeatable results,

the pressure-velocity curves for the three missile types were derived. Several missiles were fired at a specified pressure against a dampening apparatus made of several layers of ¾" plywood, and the velocities of the missiles were measured using the VMS. This procedure was repeated for each missile type (9-lb, 12-lb, and 15-lb) with a pressure range of from 5psi to 30psi (34.47kPa to 206.85kPa). Three to four firings were conducted from 5psi to 20psi with intervals of 1psi, and were conducted from 20psi to 30psi with intervals of 2psi, for a total of 127 tests. Mean and standard deviations were computed for each data point. Figure 13 through Figure 15 provide the pressure-velocity curves for the 9-lb, 12-lb, and 15-lb 2" x 4" wooden missiles, respectively. For each missile type, an analytical pressure-velocity relation was also obtained through interpolation of the mean results for each pressure value (see Figures 13-15).

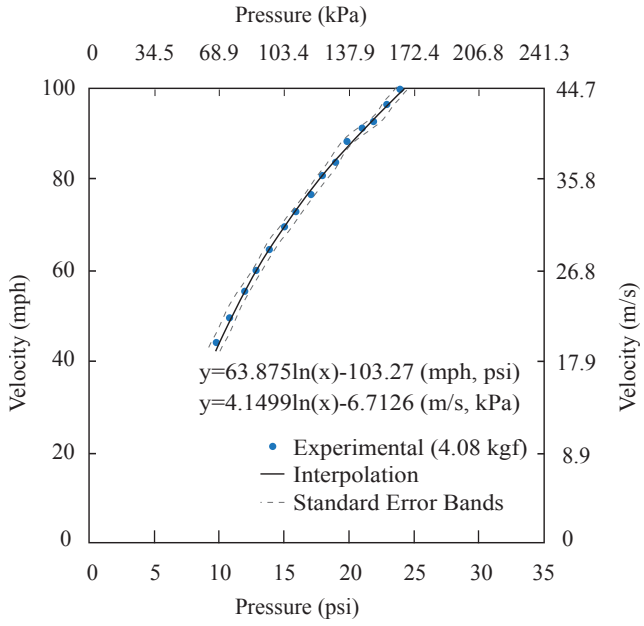

Figure 13: Pressure-velocity curve for 9-lb (4.08kg) projectiles

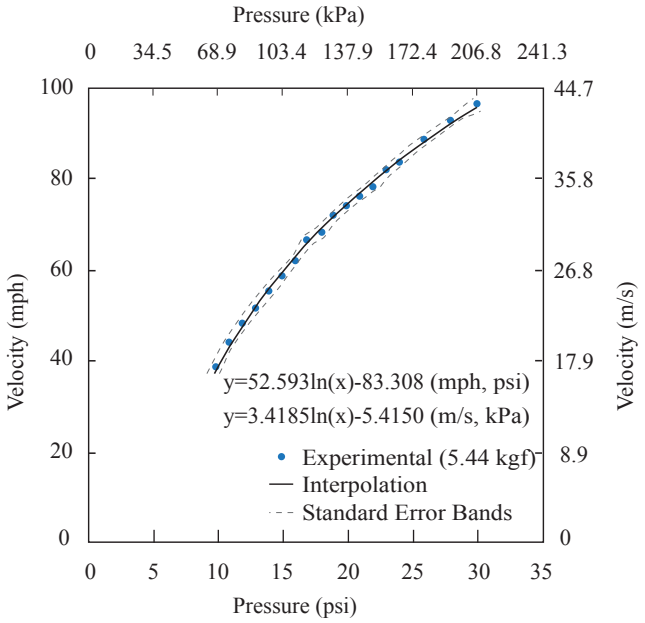

Figure 14: Pressure-velocity curve for 12-lb (5.44kg) projectiles

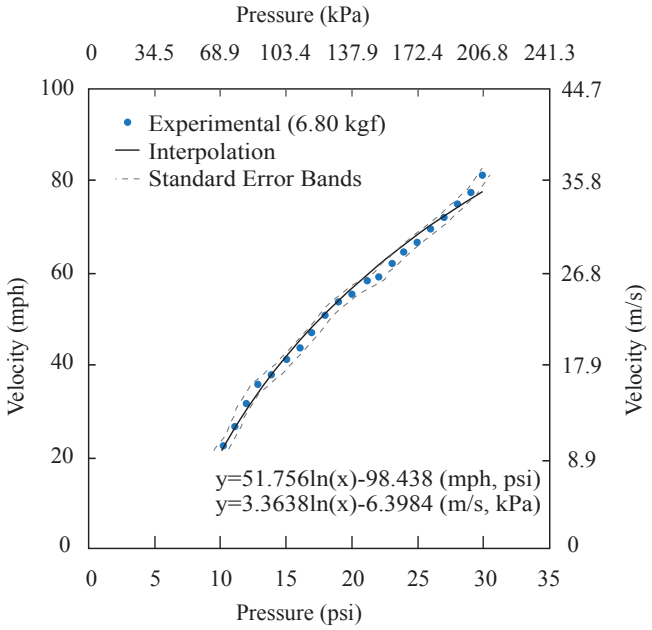

Figure 15: Pressure-velocity curve for 15-lb (6.80kg) projectiles

3.2.4. Testing Location and Equipment Storage

The testing operations for the LSU wind cannon are performed inside a standard 8’ x 8’ x 20’ shipping container located at Louisiana State University’s Blowout Prevention Facility of the LSU Department of Petroleum Engineering. This container is a very simple twofold solution, since it provides a self-contained protection system for the operators and bystanders during the testing activities, as well as a permanent storage option for the cannon to be protected from the outside environment when not in use.

3.2.5. Target Support Frame

A steel target support frame was designed to be permanently attached to the rear of the testing container while still allowing for enough space for the cannon to be stored within the container. The proposed design was analyzed using the structural engineering program ANSYS (ANSYS 2013). The target support frame was designed to withstand up to three times the predicted maximum impact force with deflections that are negligible when compared with the expected deflections of the storm panels to be tested. Figure 16 shows an Autodesk Revit Structure (REVIT 2013) model of the target support frame. The components of the frame are:

1. Standard steel shipping container
2. Left vertical support (W6x25 steel beam)
3. Right vertical support (W6x25 steel beam)
4. Top horizontal support (C6x12 steel channel)
5. Bottom horizontal support (W6x20 steel beam)
6. Top welded connection
7. Bottom welded connection

8. Container floor (wooden 2” x 6” boards)

The beams that run parallel to the ground across the front of the target support frame are the main components in this design. These members are subjected to the maximum impact load when directly hit by the projectile. In any other case, once the projectile impacts the target, the kinetic energy that is in the projectile right before impact will be partially dissipated before affecting the considered beams.

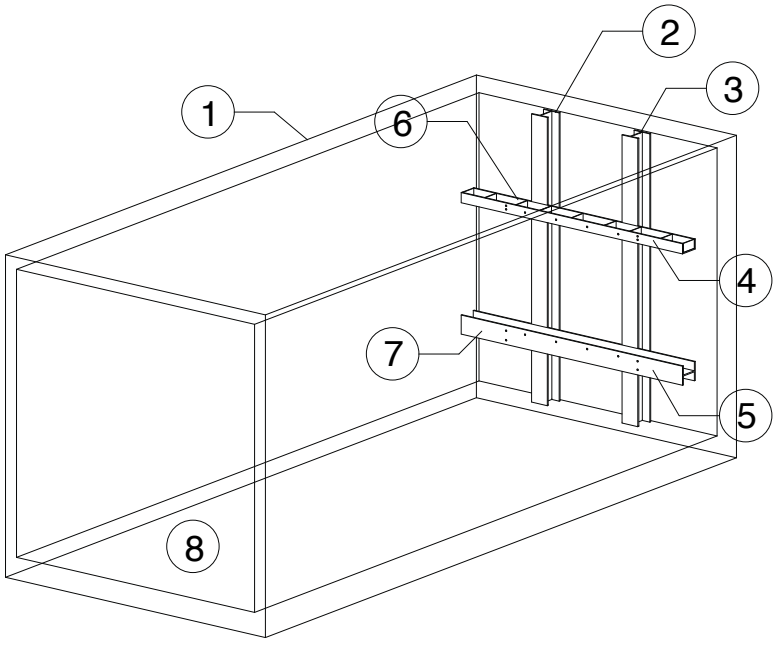

Figure 16: Target support frame description

The dimensioning of the beams was performed under the following assumptions of worst-case scenarios:

1. All of the initial kinetic energy from the projectile is transmitted into strain energy that is used to deform the crossbeam.
2. The projectile does not rebound away from the crossbeam.

3. There is no energy lost through heat transfer from the impact.
4. The crossbeams are modeled as beams with pinned-pinned end conditions.

3.2.6. Deflection Measurement System

The experimental equipment used in this research includes a measurement system for both maximum deflections and plastic deformations. The maximum deflection measurements are needed to build the fragility curve of the aluminum panels corresponding to failure of the protected window, whereas the plastic deformation measurements are needed to build the fragility curve of the aluminum panels corresponding to failure of the panel.

Plastic deformations are easily measured while the panel is still connected to the frame after the impact. Using the cross beams that the panel is bolted to, a straight beam lying vertically against the cross beams, and a square ruler, the plastic deflection is easily recorded in the units of choice.

The maximum deflection measurement system consists of aluminum (stiff) dryer vents. This measurement system was devised based on recommendations made by the Miami-Dade testing department (personal communication). Two configurations were used in the tests: (1) a single 4" dryer vent extended 75% pressing upon the rear of the panel when the exact impact location was known, and (2) multiple 2" dryer vents extended 75% pressing upon the rear of the panel when the impact location was not known exactly (e.g., random impact locations). In both configurations, the dryer vent is in the horizontal direction parallel to the projectile's travelling direction. Figure 17 shows the installation and use of a dryer vent for impact deflection measurements, as well as a graphical representation of the measured plastic deformation and maximum deflection.

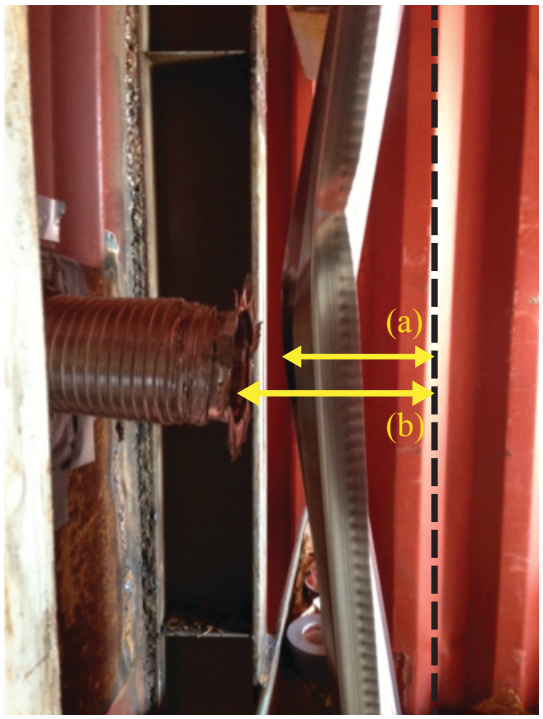

Figure 17: Dryer vent DMS: (a) plastic deformation, (b) maximum deflection

3.3. Experimental Specifications

The experimental tests for the present study were performed meeting or exceeding ASTM E1996 specifications. The following subsections summarize the ASTM specifications that are most relevant for this research.

3.3.1. Projectile Specifications

The 2" x 4" missiles used in the experiment followed the strict guidelines set forth by ASTM E1996, which were followed also for the additional missile type (i.e., the 12-lb missile), which is not included in the ASTM E1996 specifications but was considered in this study for comparison purposes with the results presented in Herbin (2011). ASTM E1996-08e1 specifies the following projectile specifications:

- *Each projectile must be weighed 15 min. prior to testing.*

- *Any soft wood lumber species as defined by the DOC PS 20 shall be permitted. It shall be of grade 2 or better and free of splits, checks, wane and any other significant defects. (ICC-500)*

- *The 2 x 4's used shall be straight such that any bow or warp measured by stretching a string or wire on the left side of the board from end to end is within 0.5 inches of the 2 x 4's surface over its entire length. (ICC-500)*

ASTM E1996-08e1 also specifies that the testing weight of the missiles stay within a +/- 0.25lb weight tolerance and the suggested length tolerance that corresponds with the respective weight (i.e., +/- 6" from 13.5' for the 15-lb missile and +/- 4" from 8' for the 9-lb missile).

3.3.2. Impact Specifications

The impact specifications from ASTM E1996 are as follows:

- *The projectile exiting chamber must be located approximately 1.5 times the projectiles length from the specimen, this length must not be less than 5.91 ft. (ASTM 1996-08e1)*

- *For missiles having a longitudinal axis, on impact the longitudinal axis of the missile must be within +/- 5 degrees of a line normal to the specimen at the impact point. (ASTM E1886-05)*

In addition, ASTM E1996 provides preferred impact locations for large and small missiles. For large missiles, such as the 2" x 4" missiles considered in this research, two different impacts are required. In the first impact, the missile should impact the target within a 5" diameter circle from its geometrical center. In the second impact, the missile

should strike the target within a 5” diameter circle with a center located 6” from the corner. Since the focus of this research was not to verify if the considered storm aluminum panels satisfy the ASTM specifications, the specifications on the preferred impact locations for the large missile did not apply to the experimental testing described in this thesis.

3.3.3. Velocity Specifications

ASTM E1996 provided the following velocity specifications for 2” x 4” missiles:

- *The projectile speed measuring device must be calibrated to within the following tolerances (ASTM 1996-08e1)*
    - *±2% specified speed when speed ≤ 75.5 ft/s*
    - *±1% specified speed when speed > 75.5 ft/s*

- *There shall be no further acceleration of the projectile when the speed measurement is taken. (ASTM 1996-08w1)*

- *The missile test speed tolerance is four mph above and zero mph below the missile speed prescribed. (ICC-500)*

- *Large missiles shall be designed to be launched at speeds between 10 and 55 percent of the specified wind speed. (ASTM E1886-05)*

The first two set of specifications were met or exceeded during the experimental testing performed in this research. The last two set of specifications did not apply to the research presented here.

3.3.4. Sabot Specifications

ASTM E1996 provides the following recommendation regarding the sabot connected to the missile:

- *Where the projectile launching system requires the use of a sabot for the effective launching of the missile, the sabot shall weigh no more than 0.50lb and shall be included in the weight of the missile, unless it is stripped away during flight prior to impact. (ICC-500)*

The sabot consists of a circular cut section of medium density fiberboard (MDF). These sabots were cut to measure exactly 5-5/8" in diameter, in order to ensure that a proper thrust was available to the projectile. These sabots were screwed onto the end of the 2" x 4" missiles and were pushed to the back of the barrel for firing (see Figure 18).

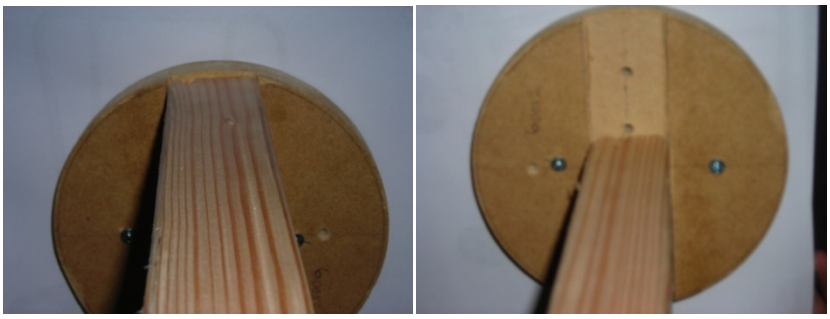

Figure 18: Sabot attachment

3.4. Procedure and Safety

As a requirement of LSU's facility services and the facility manager at the Blowout Prevention Facility, a safe procedure was developed and documented to ensure safety of the operators and of the equipment surrounding the air cannon. The full procedure, given as a list of directions, is provided in Appendix A.

This procedure was followed throughout the duration of the experimental campaign at the facility. No injuries or accidents occurred during the use of the wind cannon.

4. EXPERIMENTAL RESULTS AND DISCUSSION

4.1. Experimental Specimens: Aluminum storm panels

Numerous BEC protection options are readily available for practical applications, e.g., Bahama shutters, colonial shutters, and storm panels. For this research, corrugated aluminum storm panels were considered. These storm panels are characterized by relatively low cost, mobility, and ease of installation. The geometrical schematics for this type of hurricane protection are readily available (MSOBPC 2013). The side dimensions of the panel are height H = 47.25in (120.01cm), and width W = 14.37in (36.51cm). The aluminum panels are made of 0.05in (1.27mm) gauge 3004 H34 type aluminum. A technical drawing of the cross section and detail of the panel can be seen in Figure 19.

A picture of an aluminum storm panel is shown in Figure 20. ASTM E1996 standard specifies that this gauge aluminum storm panel should be able to withstand the impact of a 9-lb 2" x 4" missile traveling at 80ft/s (54.54mph). The panel's material properties are provided in Table 1.

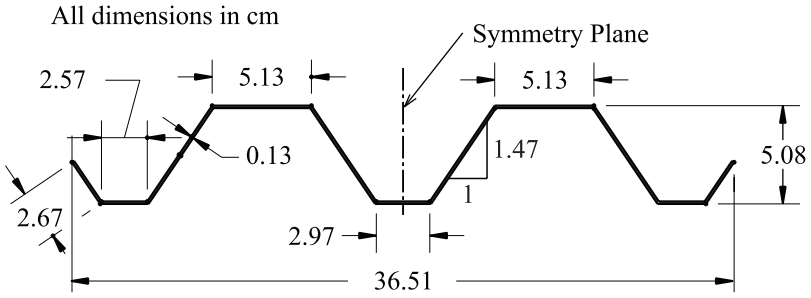

Figure 19: Aluminum storm panel technical drawings of the cross-section

Figure 20: Typical aluminum storm panel

Table 1: 3004 Aluminum Material Properties

Parameter	Value
Density (lb / cu. in.)	0.098
Specific Gravity	2.72
Melting Point (deg F)	1170
Modulus of Elasticity (ksi)	10000
Shear Modulus (ksi)	3800

4.2. Determination of a Suitable *IP*

A first set of experiments was performed to determine an appropriate *IP* for BECs with ductile behavior. The following three potential *IP*s were considered: (1) missile impact velocity, V_m, (2) missile impact linear momentum, LM_m, and (3) missile impact kinetic energy, KE_m. To evaluate the sufficiency of each *IP*, a WBD impact test was conducted using a constant impact location corresponding to the center of the panel. The

impacts occurred at various levels of the possible *IP*s, which were obtained by considering missiles of three different sizes, i.e., 9-lb, 12-lb, and 15-lb (i.e., with masses 4.08kg, 5.44kg, and 6.80kg, respectively), and several different velocities, for a total of 62 impact tests.

During each impact test, the values of the following two *EDP*s were recorded: (1) the maximum total deflection of the storm panel during impact, Δ_{max}, and (2) the plastic deflection of the storm panel after impact, Δ_{pl}. The maximum deflection Δ_{max} was considered because it is directly related to potential damage to the windows, which need to be protected by the storm panel. The plastic deflection Δ_{pl} was considered because it is directly related to potential damage to the storm panel. The values of Δ_{max} and Δ_{pl} recorded from this testing with fixed impact point near the center of the storm panels were denoted as Δ^0_{max} and Δ^0_{pl}, respectively.

The *EDP* values obtained from this test were plotted versus V_m in Figure 21, LM_m in Figure 22, and KE_m in Figure 23, in order to evaluate the sufficiency of the three potential *IP*s considered in this research. It is observed that, in the two cases where V_m and LM_m are considered as *IP*s, both Δ^0_{max} and Δ^0_{pl} present a significant scatter. In both of these cases, the *EDP*s are dependent on V_m and LM_m, with approximately a linear functional dependency, as well as the weight of the missile. The results presented in Figure 23 indicate that Δ^0_{max} and Δ^0_{pl} depend only on KE_m, whereas they are independent of the weight of the missile. The experimental results indicated also that, for an impact kinetic energy $KE_m \geq 1.150$kJ (see vertical dashed line in Figure 23, representing the

strength limit for the considered aluminum storm panel), the storm panels were significantly damaged or completely failed due to penetration of the missile or failure of the connection with the support frame. Figure 24 shows a panel failure from penetration while testing at an *IP* level of KE_m = 1.500kJ, whereas Figure 25 shows a panel failure due to tearing from the support frame at an *IP* level of KE_m = 1.175kJ. For these values of impact kinetic energy, the deflection measurements do not have the same physical meaning as for lower values of the impact kinetic energy, as demonstrated by the change in the relation between impact kinetic energy and *EDP*s.

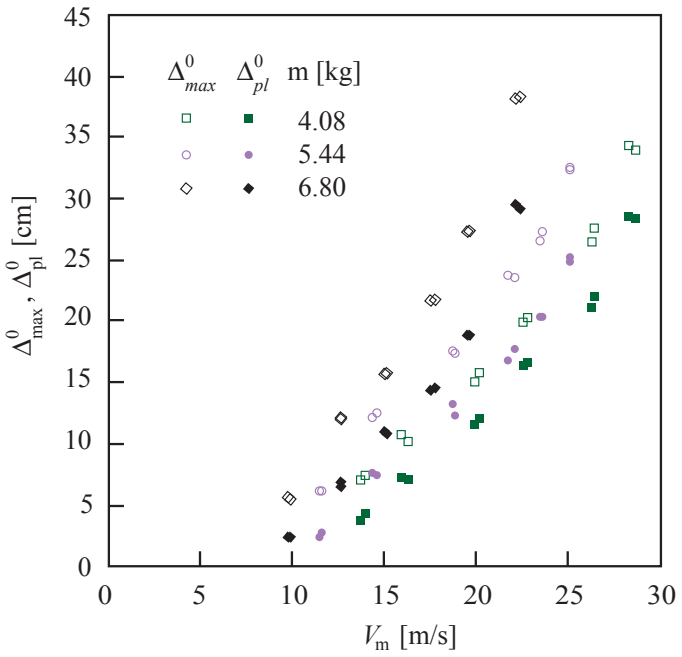

Figure 21: *EDP* values for the panel considering V_m as *IP*.

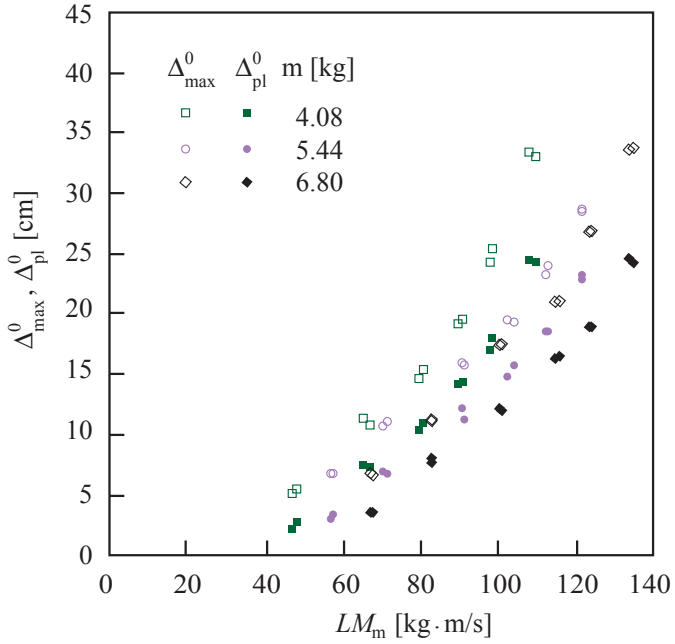

Figure 22: *EDP* values for the panel considering LM_m as *IP*.

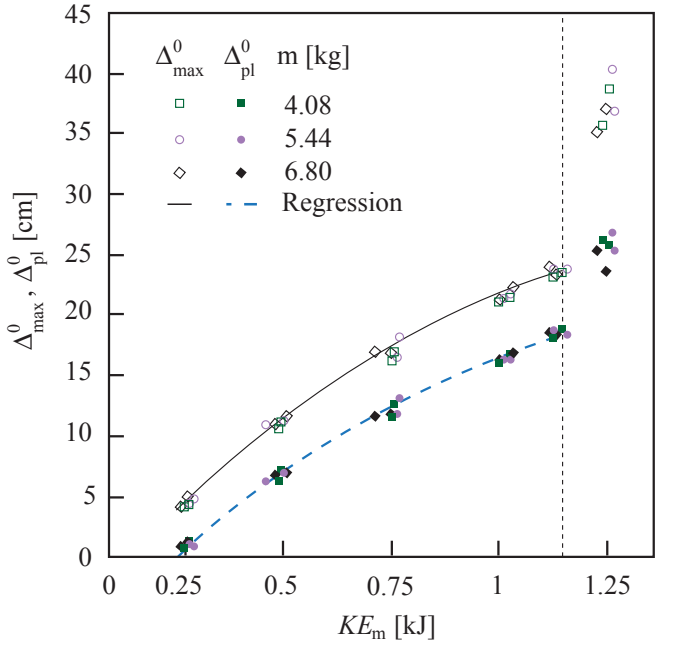

Figure 23: *EDP* values for the panel considering KE_m as *IP*.

Figure 24: Panel Failure at KE_m = 1.500kJ

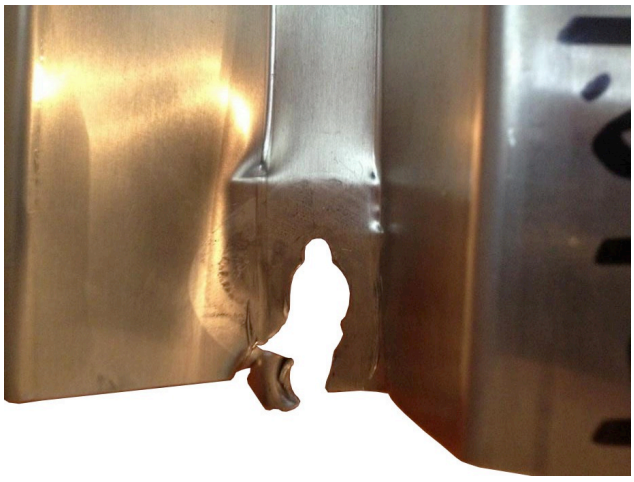

Figure 25: Panel failure due to tearing from crossbeams at bolt holes

Based on the results obtained in this first set of tests, it is concluded that KE_m is the only sufficient (and thus appropriate) *IP* for BECs with ductile behavior relative to the considered *EDP*s among the potential *IP*s investigated in this research. This

conclusion is consistent with results available in the literature (Borges et al. 2009, Herbin and Barbato 2012).

4.3. Structural Analysis Results and Statistical Characterization of the *EDP*s

The structural analysis phase of PBHE provides the statistical description of the *EDP*s conditional to the value of the identified *IP*, KE_m. An example of probabilistic structural analysis for PBHE is given by Herbin and Barbato (2012), where numerical simulation using stochastic finite element analysis is used to derive fragility curves for the same aluminum storm panels considered in this research.

A second set of tests was performed to derive the experimental fragility curve for the considered storm panel corresponding to one *IP* level, i.e., KE_m = 0.500kJ. Only one missile size was used (i.e., 9-lb missile). The impact locations were selected randomly using a uniform distribution for both horizontal and vertical coordinates. A total of 14 impact tests were performed. Due to the variability of the actual missile velocity when using the pressure-velocity curves derived for the 9-lb missile, the actual range of the measured impact kinetic energy was 0.488kJ $\leq KE_m \leq$ 0.513kJ. The boundary conditions considered in this test were bolted connections along the two shorter sides (i.e., top and bottom sides) of the storm panel and free ends along the two longer sides of the storm panel (see Figure 26). This set of tests was used to identify the different types of impacts and ultimately evaluate an experimental fragility curve for the storm panels considered in this research.

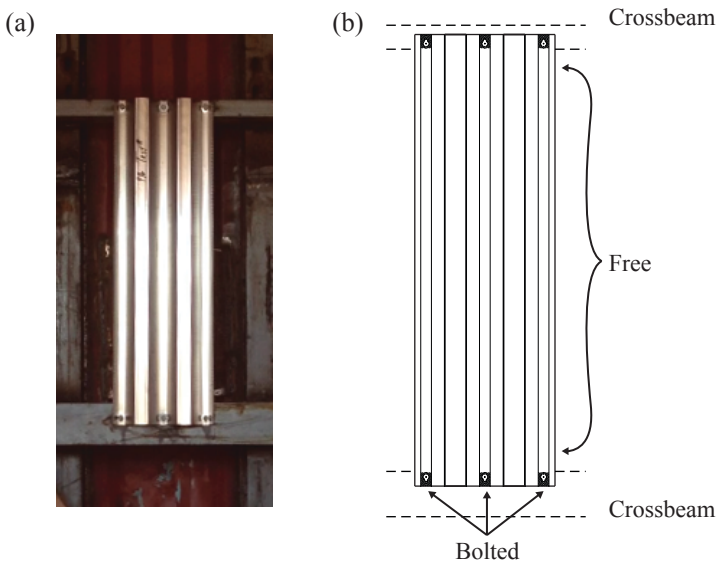

Figure 26: Experimental setup of the aluminum storm panel: (a) picture of the panel before impact, and (b) drawing of boundary conditions adopted as reference installation during impact testing.

Figure 27 and Figure 28 plot the experimental CDFs for Δ_{max} and Δ_{pl}, respectively, for the KE_m level of 0.500kJ. These two experimental curves provide the probabilistic information needed to describe the limit states of damage to the panel, damage to the window, and penetration.

4.3.1. Identification of Impact Typologies

The following three different response regions can be identified in the experimental CDFs plotted in Figure 27 and Figure 28: (1) a region with a concentration of very small values of Δ_{max} and Δ_{pl}, corresponding to "boundary impacts", (2) a region with values of Δ_{max} and Δ_{pl} that are more evenly distributed, corresponding to "ordinary impacts", and (3) a region where the missile penetrated the aluminum storm panel,

corresponding to “penetrations”. These experimental results were qualitatively consistent with the numerical results presented in Herbin and Barbato (2012).

The measurements of Δ_{max} and Δ_{pl} corresponding to penetrations do not have the same physical meaning as for boundary and ordinary impacts. Thus, using an approach commonly employed in other performance-based engineering frameworks, an infinite value of maximum and plastic deformation was associated to penetration events, for which only their number was recorded experimentally (see Figure 27 and Figure 28, where three penetrations were recorded).

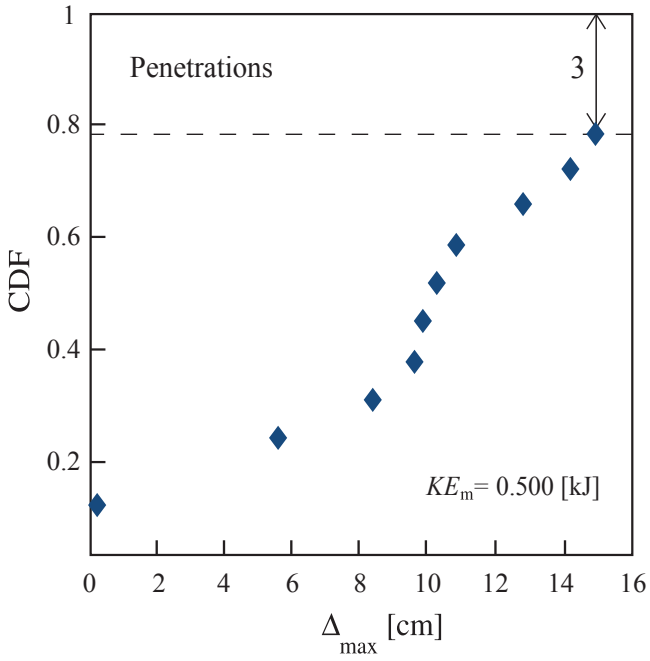

Figure 27: Experimental CDF for Δ_{max} including all types of impacts at randomized locations.

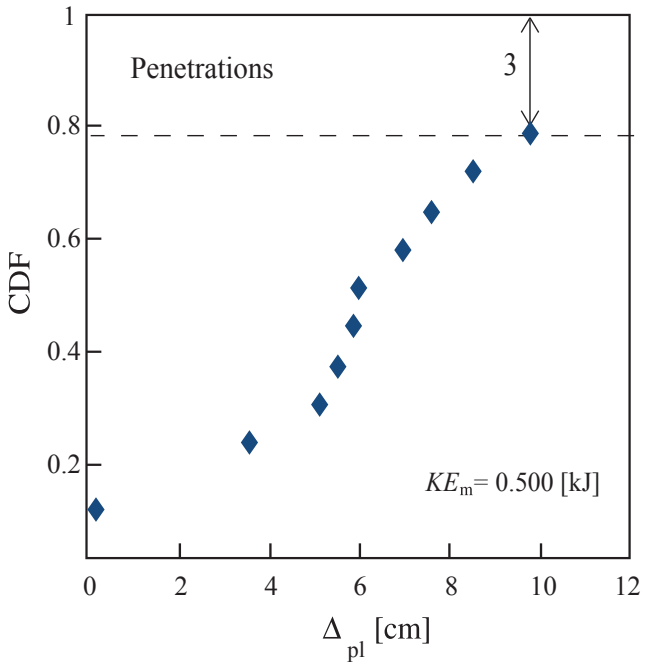

Figure 28: Experimental CDF for Δ_{pl} including all types of impacts at randomized locations.

The results presented in Figure 27 and Figure 28 can be better understood by analyzing the WBD impact locations shown in Figure 29 and the corresponding impact characteristics. Figure 29 shows the locations of the impacts and their classification into boundary impacts, ordinary impacts, and penetrations. It also identifies the regions where the three types of impacts are most likely to happen.

When the impact locations occur in the portion of the aluminum storm panel that is connected to the frame, as well as in an additional region that extends from the short side boundary connections by half of the height of the 2” x 4” missile (i.e., 4.445cm), the projectiles impact the support frame.

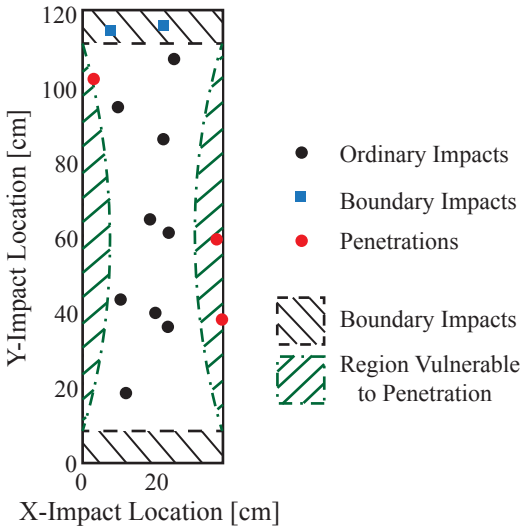

Figure 29: Impact locations and corresponding impact types for KE_m = 0.500kJ.

If the frame is significantly stiffer than the panel (which is the common condition for almost all residential construction), the values of Δ_{max} and Δ_{pl} are very small because they are limited by the presence of the frame (Herbin and Barbato 2012). These conditions, originally suggested in order to explain numerically derived fragility curves (Herbin and Barbato 2012), were observed and verified experimentally in this research, as shown in Figure 27 and Figure 28. These boundary conditions result in a net reduction of the vulnerable area of the panel. The *EDP* values for these impacts typically depend on the properties of the structural component on which the storm panel is installed.

The results presented in Figure 29 show that the impact locations corresponding to penetrations are concentrated in the portions of the aluminum storm panel that are located near the unconstrained sides. These portions can be approximately identified with two symmetric parabolic segments with base b = 103.51cm and height h = 6.35cm. The total sum of these two parabolic areas consists of nearly 20% of the total panel area,

which is very close to the ratio between the number of penetrations and total number of impact analyses obtained in this research (i.e., 21.4%, with 3 penetrations out of 14 random impacts). These results are also consistent with those presented in Herbin and Barbato (2012), where the same portions of the aluminum storm panel were identified as vulnerable to penetration and similar values of the probability of penetration were obtained (20.8%, with 125 penetrations out of 600 finite element simulations). Thus, the experimental results obtained in this research confirm that the probability of penetration for an aluminum storm panel is strongly dependent on the boundary conditions (i.e., on the connection details).

When the impact occurs in the portion of the panel that is not on the boundary connection or in the region vulnerable to penetration, an ordinary impact is expected, for which finite *EDP* values are obtained that are typically larger than those corresponding to boundary impact. For ordinary impacts, it is of interest to identify appropriate probability distributions that can be used to describe the fragility curve corresponding to the limit states of damage to the panel and to the window.

4.3.2. Statistical Characterization of the *EDP*s for Ordinary Impacts

Experimental CDFs were obtained considering only the values of the *EDP*s obtained from ordinary impacts (i.e., not including the results that corresponded to boundary impacts and/or penetrations) and normalizing the probability of those results to one. From these values, the means and standard deviations for Δ_{max} and Δ_{pl} were computed. The normal, lognormal, and truncated normal (with lower truncations at Δ_{max} = 0cm and Δ_{pl} = 0cm) distributions were compared in order to find the best fit to the

ordinary impacts' results. The comparison of these distributions was based on the modified Kolmogorov-Smirnov goodness-of-fit test (Kececioglu 1993). Figure 30 and Figure 31 illustrate the experimental CDF for Δ_{max} and Δ_{pl}, respectively, along with the theoretical CDFs for all considered distributions, corresponding to $KE_m = 0.500$kJ (i.e., 9-lb missiles impacting at 35.011 mph).

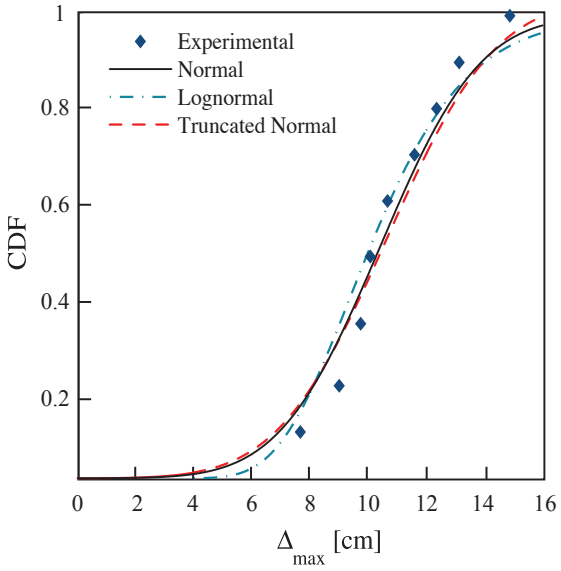

Figure 30: Experimental and theoretical CDFs of Δ_{max} for randomized ordinary impacts and $KE_m = 0.500$kJ.

In the modified Kolmogorov-Smirnov test, the proposed distribution is accepted at a given significance level, α, if the maximum difference between the experimental CDF and the theoretical CDF, D_n, is less than the critical value, $D_{n,\alpha}$, corresponding to the given level of significance (Ang and Tang 1975). In Herbin and Barbato (2012), the lognormal distribution was excluded as a possible fit for the data, and the truncated normal distribution was preferred over the normal distribution.

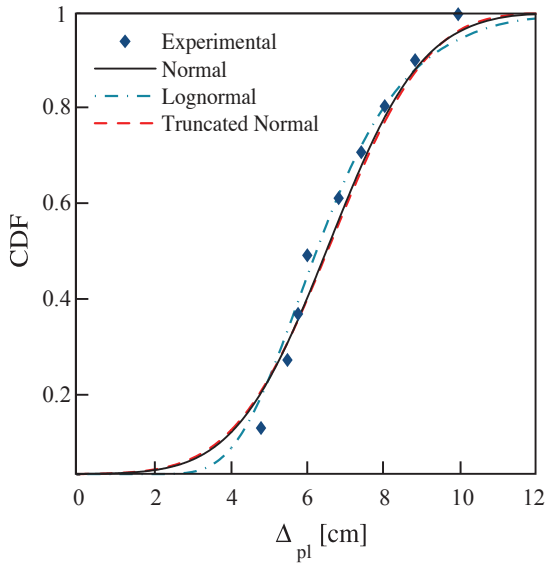

Figure 31: Experimental and fitted CDFs of Δ_{pl} for randomized ordinary impacts and $KE_m = 0.500$kJ.

Table 2 provides the results of the modified Kolmogorov-Smirnov test corresponding to the $KE_m = 0.500$kJ data with significance levels α = 5% and α = 1%. The critical $D_{n,\alpha}$ values were obtained from Kececioglu (1993). In Table 2, bolded D_n values indicate that the considered probability distribution is acceptable at α = 5% significance, and underlined D_n values indicate that considered probability distribution is acceptable at α = 1%.

Table 2: Modified Kolmogorov-Smirnov test results for the probabilistic characterization of the EDPs corresponding to ordinary impacts.

KE_m [kJ]	N	Observed D_n ($\Delta_{max} - \Delta_{pl}$)			Critical D_n	
		Distribution			α	
		Normal	Lognormal	Truncated Normal	.05	.01
0.50	9	0.469-**0.423**	0.588-0.547	**0.430**-**0.412**	0.432	0.514

It is observed that the truncated normal distribution is acceptable at α = 5% significance for both *EDP*s considered in this study, the normal distribution is acceptable at α = 1% significance for Δ_{max} and at α = 5% significance for Δ_{pl}, and the lognormal distribution is not acceptable at α = 1% significance for either Δ_{max} or Δ_{pl}. Thus, the truncated normal distribution is preferred over the normal distribution as it avoids physically impossible negative values of Δ_{max} and Δ_{pl}. This result is consistent with Herbin and Barbato (2012).

4.4. Effects of Boundary Conditions

The effects of different boundary conditions on the performance of aluminum storm panels were studied by conducting repeated impact tests at specified *IP* levels. In this test, two different installation options were considered: (1) a reference installation option in which the aluminum storm panel does not have any support on the two long sides (shown in Figure 26 and corresponding to cases in which the panel is not wider than the opening to be protected), and (2) a new installation option in which the panel can receive some support on the long sides (shown in Figure 32 and corresponding to cases in which the panel is wider than the opening to be protected). The new boundary conditions replicate the manufactured-suggested mounting on a fixed rail system with a panel that overlaps the installation wall by 1.270cm along the two unconstrained sides of the panels (i.e., the portions of the panel that are most vulnerable to penetrations). Installation of panels using these new boundary conditions assumes that the wall is sufficiently strong to tolerate impact without damage (which is a reasonable hypothesis for brick and/or concrete walls). In order to represent this condition during testing, a steel plate was used to

provide the support corresponding to the installation wall. It is noteworthy that both installation options are acceptable according to manufacturer's suggestions and code prescriptions, assuming that the distance between the panel and the side of the opening to be protected is smaller than ¼" (6.35mm).

This experimental test consisted of a total of 32 impact tests with random impact locations that were selected within the parabolic regions considered prone to penetration for each of the two installation options (see Figure 32), as identified in Herbin and Barbato (2012). In particular, 16 impact tests were conducted at KE_m = 0.250kJ (actual variability: 0.238kJ ≤ KE_m ≤ 0.256kJ), and 16 impact tests were conducted at KE_m = 0.500kJ (actual variability: 0.491kJ ≤ KE_m ≤ 0.520kJ) using a 9-lb missile.

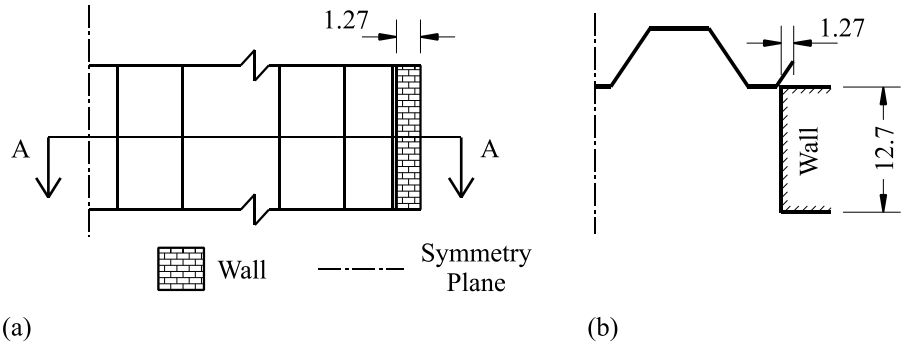

Figure 32: New boundary condition case corresponding to an aluminum storm panel wider than a window opening: (a) elevation, and (b) section

Figure 33 shows the impact locations and the corresponding impact types for KE_m = 0.250kJ, as well as the parabolic regions vulnerable to penetration for (a) the reference boundary conditions, and (b) the new boundary conditions. Figure 34 provides the same information as Figure 33 for KE_m = 0.500kJ.

In the first set of 16 impacts considering the reference boundary conditions, all impacts occurred within the two symmetric parabolic regions, which were identified as

the storm panel's regions that are most vulnerable to penetration. In this first set of tests, a total of 15 penetrations were recorded. Eight penetrations were recorded for KE_m = 0.250kJ, corresponding to a probability of penetration conditional to impact occurring in the region vulnerable to impact (in short, conditional probability of penetration) equal to 100%, and seven for KE_m = 0.500kJ (corresponding to a conditional probability of penetration equal to 87.5%). In the second set of 16 impacts considering the new boundary conditions, 15 impacts occurred within the parabolic regions identified as vulnerable to penetration (one of which was the only actual penetration recorded), and one was a boundary impact on the boundary of the panel's long dimension, which is supported by the installation frame for the new boundary conditions. For this second set of tests, no penetration was recorded for KE_m = 0.250kJ, and only one penetration was recorded for KE_m = 0.500kJ, out of seven impacts occurring in the vulnerable region of the panel (corresponding to a conditional probability of penetration equal to 14.3%). These results are qualitatively consistent with those reported in Herbin and Barbato (2012), where the comparison between the same two installation options considered in this study was performed based on numerical simulation. In their study, for an impact kinetic energy KE_m = 1.088kJ, it was found that (1) 19 out of 21 impacts located in the parabolic regions vulnerable to penetration resulted in penetrations for the reference boundary conditions (i.e., corresponding to a probability of penetration conditional to impact on vulnerable regions equal to 90.5%), and (2) three out of six impacts located in the parabolic regions vulnerable to penetration resulted in penetrations for the new

boundary conditions (i.e., corresponding to a probability of penetration conditional to impact on vulnerable regions equal to 50%).

The large reduction in number of penetrations observed in this study is very significant as it can be achieved via a small modification of the installation of the panel when protecting BECs. Thus, this installation modification can be easily implemented into practical installation applications by introducing it into building code's minimum requirements, i.e., by requiring a minimum value of overlap between walls and storm panels. With this modification, the region of the storm panel where boundary impacts take place becomes significantly larger than the region identified in the reference installation option. This new boundary region includes not only the boundary impact areas located at the top and bottom of the panel near the bolted connections with the fixed rail, but also two additional side regions along the unconstrained sides of the panel, which have a width equal to the width of the overlap between the wall and the storm panel plus one half of the missile width. In addition, the results presented in Figure 33 and Figure 34 suggest that penetrations of the storm panels are strongly dependent on the missile's impact location and panel's boundary conditions. Both of these figures exemplify the three types of impacts (i.e., ordinary impacts, boundary impacts, penetrations). The figures also identify the unique regions on the panel that are likely to cause boundary impacts (impacts causing little to no deflections), and the region vulnerable to penetrations (impacts that cause the panel to act in a "push-out" manner allowing for the projectile to pass the specimen and cause damage to the window or element located behind the aluminum storm panel).

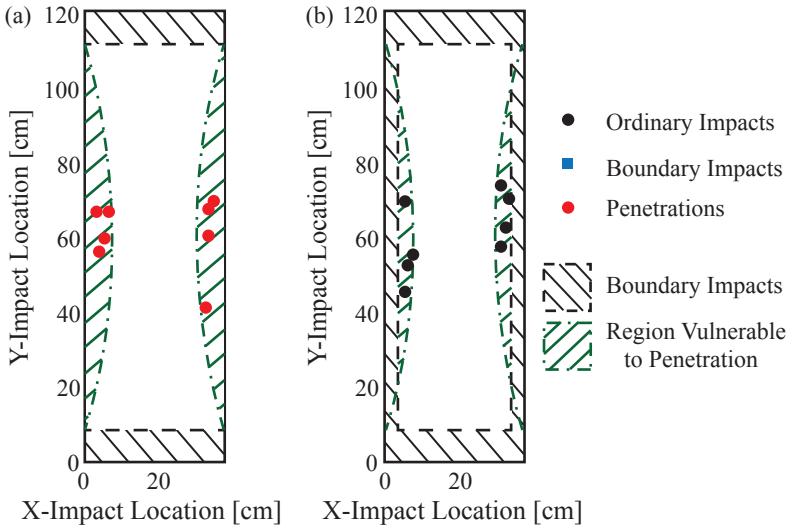

Figure 33: Impact locations and corresponding impact types for $KE_m = 0.250$kJ: (a) reference boundary conditions (b) New boundary conditions.

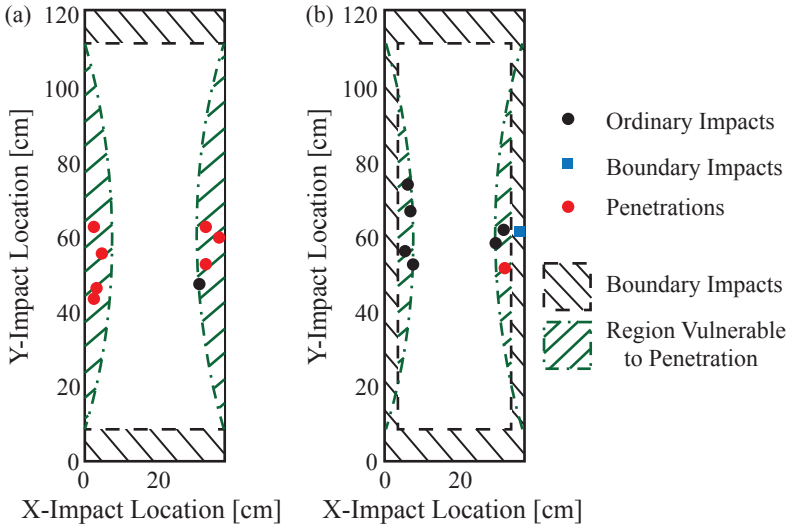

Figure 34: Impact locations and corresponding impact types for $KE_m = 0.500$kJ: (a) reference boundary conditions, and (b) new boundary conditions.